Dup

FINAL PROJECT REPORT SERDP PROJECT CS-1142
Interim Progress Report and Final Report for
ARO Grant Number DAAD-19-99-1-0261

"DIRECT DETECTION OF ARCHAEOLOGICAL SITES USING REMOTE SENSING"

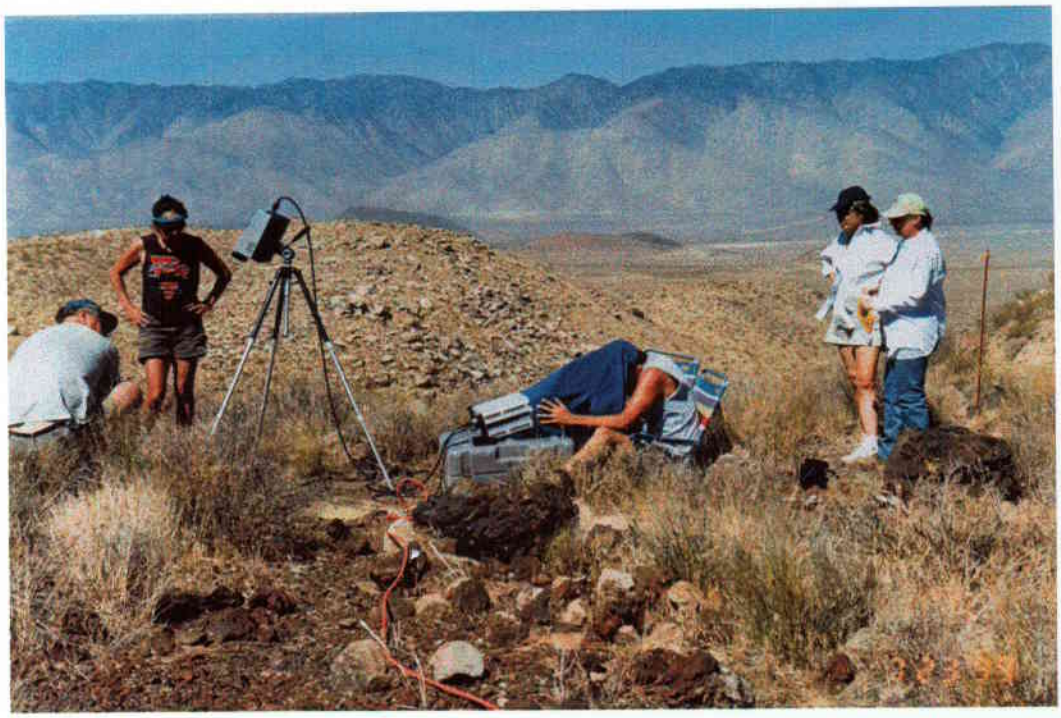

D. Sabol, P. Buck, and A. Gillespie

Desert Research Institute and University of Washington

April 12, 2000

Report Documentation Page

Form Approved
OMB No. 0704-0188

1. REPORT DATE	2. REPORT TYPE	3. DATES COVERED
12 APR 2000		**00-00-2000 to 00-00-2000**

4. TITLE AND SUBTITLE	5a. CONTRACT NUMBER
Direct Detection of Archaeological Sites Using Remote Sensing	5b. GRANT NUMBER
	5c. PROGRAM ELEMENT NUMBER
6. AUTHOR(S)	5d. PROJECT NUMBER
	5e. TASK NUMBER
	5f. WORK UNIT NUMBER
7. PERFORMING ORGANIZATION NAME(S) AND ADDRESS(ES) **Desert Research Institute,2215 Raggio Parkway,Reno,NV,89512**	8. PERFORMING ORGANIZATION REPORT NUMBER
9. SPONSORING/MONITORING AGENCY NAME(S) AND ADDRESS(ES)	10. SPONSOR/MONITOR'S ACRONYM(S)
	11. SPONSOR/MONITOR'S REPORT NUMBER(S)

12. DISTRIBUTION/AVAILABILITY STATEMENT
Approved for public release; distribution unlimited

13. SUPPLEMENTARY NOTES

14. ABSTRACT

15. SUBJECT TERMS

16. SECURITY CLASSIFICATION OF:			17. LIMITATION OF ABSTRACT	18. NUMBER OF PAGES	19a. NAME OF RESPONSIBLE PERSON
a. REPORT **unclassified**	b. ABSTRACT **unclassified**	c. THIS PAGE **unclassified**	**Same as Report (SAR)**	**36**	

Interim Progress Report and Final Report for **ARO** Grant Number DAAD19-99-1-0261
Final Report for **SERDP** Project Number CS-1142

"DIRECT DETECTION OF ARCHAEOLOGICAL SITES USING REMOTE SENSING"

D. Sabol[1], P. Buck[2], and A. Gillespie[2]

Introduction

The research described here was conducted in response to Broad Agency Announcement 98-003 for FY 1999 Strategic Environmental Research and Development Program (SERDP). Specifically, it partially addresses Statement of Need (SON) Number CSSON-99-01, "Cultural Resources Management Detection and Evaluation Technologies." The objective of this statement of need is to improve the identification and assessment of prehistoric, historic, and traditional cultural properties for sites on Department of Defense (DOD) and Department of Energy (DOE) lands. The SON also identifies other needs, including more efficient information management technologies, and sharing of tools, data, and other resources with appropriate users. This study is designed to partially address that need by examining whether certain kinds of archaeological materials may be detected remotely.

The central purpose of this study is to evaluate the spectral detectability of selected types of prehistoric artifacts common at archaeological sites of the Southwestern United States using remote sensing. The ground surface at any given archaeological site or other location is composed of a number of natural and man-made materials, including soil, rock, vegetation, and artifacts. A spectrum collected by a sensor is a combination of the individual spectra of these materials such that, as the percent composition of a material on the surface increases, its spectral representation in the mixed spectrum increases. Even if a material has a its own unique spectrum, it's representation in the mixed spectrum may be very subtle, unless it comprises a significant portion of the surface.

Spectral detectability of target materials is affected by many factors, including: 1) the spectral contrast between the target and background materials, 2) the proportion of the target on the surface (relative to background), 3) the imaging system being used (bands, instrument noise, pixel size), and 4) the conditions under which the surface is being imaged (illumination, atmosphere). A detection threshold is defined as the minimum amount of target material that must be present for it to be detected at a given probability. This threshold holds for any pixel size. Whatever the pixel size, the surface area on the ground, represented by an image pixel, must have at least a certain fraction of exposed target to be detected. That fraction is the "detection threshold."

In this study, we determine the detection thresholds for obsidian and ceramic artifacts against typical backgrounds found at study sites in two locations: 1) the Mojave Desert of the China Lake Naval Air Weapons Station (CLNAWS), California (archaeological obsidian), and 2) the Pajarito Plateau on Los Alamos National Laboratory (LANL), New Mexico (pottery sherds).

Background

A number of federal laws, including the National Historic Preservation Act (NHPA), require federal agencies to identify and evaluate archaeological and historic properties found on their jurisdictions. Federal agencies are also legally bound to take into account cultural resources which might be affected by undertakings on their lands. Conventional archaeological inventory of lands is accomplished by teams of archaeologists conducting pedestrian survey, systematically examining selected tracts, blocks, or proposed areas of disturbance. This requirement for complete inventory is often feasible when the project area is small, but when tens of millions of acres are involved, pedestrian survey is time consuming, expensive, and may adversely affect vital DOD/DOE missions. The SON identified a need for DOD and DOE to develop more cost-effective methods of conducting archaeological inventory as a primary goal.

Although remote sensing approaches have been applied to archaeological inventory problems, in the past these approaches have not met with wide success. Remote sensing in archaeology during the last two decades has involved the use of aerial photographs and photogrammetry, land cover classification, and stratification of research regions for sampling (see review in Ebert and Lyons 1983). Some applications employed digital multispectral imagery to examine environmental variables at the locations of archeological sites or to construct probabilistic models of site location (Custer et al. 1986). Seldom have these approaches considered the possibility that archaeological materials may be directly detectable, presuming that archaeological sites are too small to be resolved.

Other disciplines have used remote sensing approaches more effectively (Vincent 1997). Using both portable field spectrometers and laboratory spectrophotometers, spectra of rock, mineral, soil, and vegetation have been collected, both in the visible and near infrared (VIS/NIR) from ~.40 to 2.5 micrometer (μm) and the thermal infrared (TIR) from 3 to 14 μm. In many cases, the slopes of the spectral curves and absorption features at specific wavelength bands are diagnostic of specific minerals (Kahle and Goetz 1983, Hunt and Salisbury 1970, Hunt et al. 1973), rock types (Davis et al. 1987), or vegetation types (Justice et al. 1985, Tucker et al. 1986, Ustin et al. n.d., Elvidge 1990). Since the mid 1960s, geologists and others have exploited spectral differences of surface materials to interpret multispectral aircraft and satellite images of terrestrial surfaces. These applications are successful in part because they demonstrate a physical relationship between actual materials on the ground surface and spectral properties as measured by airborne and satellite platforms.

Multispectral images may be modeled successfully as mixtures of relatively few spectral endmembers, each of which corresponds to a significant scene component (Adams et al. 1986, Gillespie 1992, Sabol et al. 1992). In spectral mixture analysis, the scene is understood to consist of a few spectrally unique endmembers or components, which depend on the nature of the scene, as well as the spatial scale, spectral resolution, and number of bands in the image. One key notion is that there is some degree of spectral contrast between the target materials and the backgrounds, and that the

measurement instrument collects data at those bands of the spectrum which best allow discrimination between the two.

This technique, first applied to a Viking Lander I image of the Martian surface (Adams et al. 1986) is conceptually different from previous approaches in archaeology to interpreting multispectral images. This powerful new technique, which directly models image variation as combinations of laboratory spectra of actual materials, has yet to be fully applied to archaeological materials, although some preliminary steps have been taken in this direction (Buck et al. 1986a, 1986b). Results were hampered at the time by the relatively poor spatial resolution of satellite platforms and limited by the few broad bands available on Landsat to discriminate materials. Additionally, this early effort concentrated on the VNIR portion of the spectrum, where spectral contrast is minimal. Nevertheless, this work suggested that a variety of archaeological materials from a study site in the Nile Valley of Egypt might have adequate spectral contrast to be distinguished from commonly occurring background material such as dune sand and vegetation.

In the arid West, the bulk of artifacts from archaeological sites were manufactured from naturally occurring rock such as obsidian, chert, or other knappable stone. Pottery was manufactured using a combination of clay and temper which was then fired. Like many geological materials, the spectra of these commonly occurring archaeological materials may also be diagnostic, and hence identifiable using remotely sensed data. Another common artifact type in the southwestern U.S. is pottery. Pottery may be distinguishable in the thermal range from other materials because of its distinct emissivity characteristics. These potentially useful spectral attributes of artifacts make it at least theoretically possible to identify them using appropriate remotely sensed data.

The focus of the research proposed here is to determine if archaeological materials of interest are detectable given the characteristics of the measuring instruments and spectral contrasts between targets and typical backgrounds. Factors that are likely to determine whether remote sensing application of this approach will work include the radiometric, spectral and spatial resolution of the measuring instrument; the spectral contrast between targets and representative backgrounds; and the density of surface artifacts at archaeological sites.

If certain kinds of artifacts can be discriminated from spectra of background materials, then subsequent work may demonstrate that these differences can be used to interpret imagery data and remotely map archaeological sites. If target materials cannot be distinguished, then further work will be unproductive until instrumentation improves and better mathematical models are constructed.

Ultimately, a number of critical tasks will be required to resolve this problem. These include modeling of detection limits, modeling the effects of multiple scattering, construction of image spectral endmembers, model validation and finally extension of the model to larger study areas. The first critical task in this sequence, and the one we describe here, is modeling detection limits. Before describing the model and using spectral data developed for this research, we descibe our study sites and methods below.

Methods

The purpose of this research is to investigate whether selected archaeological materials (obsidian and ceramic artifacts) can be spectrally distinguished from typical backgrounds. Field spectra of typical backgrounds and targets were collected; samples of targets and backgrounds were retrieved and analyzed in the laboratory; and a detection limits model is used to determine threshold detection limits. These spectra are used in an approach developed by Sabol et al. (1992) to determine the detection threshold of these targets against various backgrounds.

Our investigations involved both laboratory and field data collection. The primary goal of data collection was to learn the spectral properties in the VIS/NIR and TIR region of obsidian and ceramic artifacts and typical background materials for the selected study sites. To model detection limits it is necessary to generate data on the spectral characteristics of background and target materials. The detection limits modeling procedures require that a representative suite of backgrounds be characterized, and then mixed in varying combinations to represent as closely as possible naturally occurring ground surfaces which might contain archaeological "targets." Spectral data of target and background materials was collected at study sites described below in the TIR and VIS/NIR. VIS/NIR band encompasses the range of ~0.4 to 2.5 μm , with the TIR extending from 3 to 14 μm.

Collection of Spectral Data

Spectra were collected in the field and also in the laboratory. In the field, thermal FLIR (Forward Looking Infrared Radiometer) images of the sites were taken using a hand-held three-channel thermal imaging system manufactured by FLIR Systems Incorporated (FSI) and specially modified by the University of Washington Geological Sciences Remote Sensing Laboratory (UWGSRSL). . For the CLNAWS study sites, thermal data were collected in three bands centered on 8.214 (Band 2), 8.654 (band 0), and 11.727 (band 1) microns. To optimize filters for obsidian and pottery, new filters were installed for the LANL sites. Bands selected were 8.518 (band 0), 9.114 (band 1), and 10.799 (band 2). Unfortunately, JPL's Prototype and Designs, Inc. Field Fourier Transform Infrared Spectrometer (μFTIR), which we had planned to use to take thermal field spectra, was unavailable during the time of our field work.

The FLIR is mounted on a tripod with a field of view directed almost straight down. When mounted about 1.6 m high, the field of view (FOV) covers somewhat less than 1.0 m^2. The FOV was marked on the ground with flagging tape by looking at the computer monitor while the FLIR is in operation. A standard 35 mm photograph was taken of the FOV in order the scale the image (i.e., figures earlier of the study plots). The imaging camera is linked with a computer and monitor that allow previewing of the data; images are saved on 3.5" floppy diskette or hard drive. Power is supplied to the system either 115AC from a generator or via 12V battery. FLIR digital data can be displayed as images using a variety of commercially available software packages including Adobe PhotoShop™ and Canvas™.

In-field VIS/NIR spectral properties of backgrounds and targets were recorded using an Analytical Spectral Devices FieldSpec Pro (ASD, Inc.) portable field spectrometer (**Figure 1**). The instrument was calibrated at the start of each session with a white reference reflectance panel. Spectral resolution of this system is 3-10 μm between 350-2500 μm resulting in 1512 channels in this range. Targets include obsidian and ceramic artifacts; backgrounds included soil, dry and fresh vegetation, rocks, and other common material in the FOV. Spectra were collected using a fiber optic "gun" or wand pointed directly at each target or background with the 25 degree FOV of the instrument focused exclusively on individual objects. Digital data were saved on the integrated computer and downloaded for subsequent analyses.

Photographs of artifact were also taken in their undisturbed setting

Thermal and VIS/NIR spectra were also collected in the laboratory. A variety of rocks, soils, and vegetation were collected from near archaeological sites felt to be representative of the materials occurring on archaeological sites. Similarly, artifacts, both lithic and ceramic were analyzed. Since we could not collect artifacts directly from archaeological sites (such collections require special permits and were not felt necessary), we borrowed a small collection of ceramic and lithic artifacts housed at LANL. Thermal spectra were collected at JPL using a Nicolet Spectrometer. VIS/NIR spectra were collected at UWGSRSL using a Perkin Elmer 19 DM spectrometer. This instrument is an all-reflecting system capable of measuring 300 – 3200 μm in 0.2-20 μm intervals. Samples were not ground or treated in any way, merely held in the optical path using sample cell holders.

Description of study sites

Study areas were selected for a variety of reasons, both pragmatic and scientific. These include: abundance of targeted materials (obsidian and ceramic artifacts), paucity of obscuring vegetation, likelihood of a variety of soil geomorphic units, availability of large scale land cover mapping using remotely sensed data, past field experiences in regions with similar physiographic characteristics (Mojave Desert and New Mexico), and discussions with land managers to resolve access and other issues. Note that the targeted materials were selected for two reasons: (1) abundance of these materials on archaeological sites in the semi-arid West, and (2) the potential for these materials to have unique spectral signatures.

We recognize that these sites might not represent typical archaeological sites in either environment. However, the sites were intentionally selected to provide a best-case test of remote sensing capabilities. If it can be shown that these large sites are detectable using best-available instruments and mathematical models, the analyses can be refined to establish detection limits, and the results applied to a wider range of archaeological occurrences. The study areas were also selected to represent a diversity of soil geomorphic types and vegetation associations.

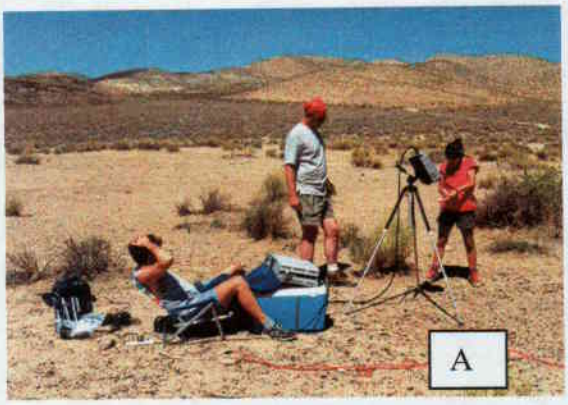

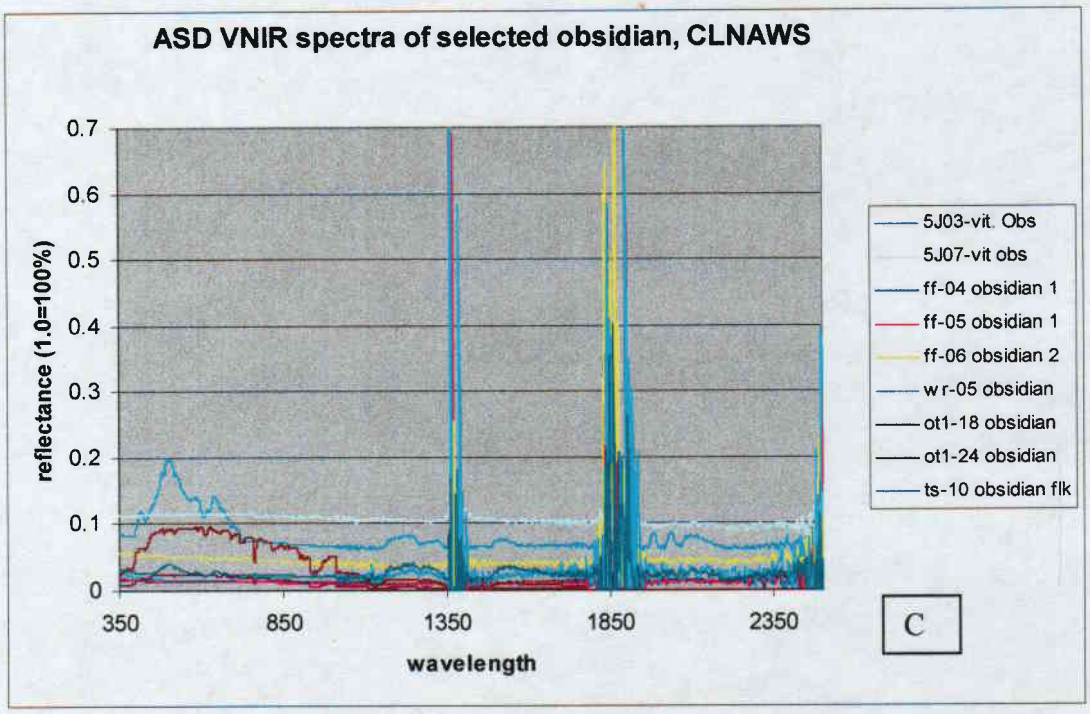

Figure 1. Remote sensing field crew in operation (A). Instrument on tripod at right of image is the FLIR. It is pointed down at a study plot 5J at China Lake Naval Air Weapons Station, California. (B) shows the operation of the fiber optic "wand" attached to the ASD field spectrometer. Spectra are being recorded of an obsidian flake. (C) Spectra of obsidian artifacts derived from ASD. The pronounced spikes in reflectance are due to absorption by water.

Study areas have been selected at CLNAWS in southeastern California (**Figure 2**) and LANL in northern New Mexico (**Figure 3**). Archaeological sites on CLNAWS are well known for huge obsidian quarries near Sugarloaf Mountain, Cactus Peak, and Coso Wash (Gilreath and Hildebrandt 1997, Hughes 1988, Elston and Zeier 1984) and non-quarry scatters. Some of these cover areas in excess of square miles and contain tens of thousands of obsidian artifacts.

Archaeological sites of the prehistoric Anasazi culture are widely distributed on LANL, and its northern border abuts Bandolier National Monument, designated as such for its remarkable prehistoric ruins. Archaeological sites containing abundant pottery and other artifacts are abundant generally on LANL, especially at Otowi Ruins (S. Hoagland, Staff Archaeologist LANL, personal communication 1998). Importantly for our purpose, the study areas have been surveyed completely by archaeologists and archaeological sites accurately mapped.

Preliminary inspection of geological maps of CLNAWS and discussions with base personnel (Carolyn Shepherd, Environmental Manager CLNAWS, personal communication 1998) suggests that the area around Sugarloaf Mountains and Cactus Peak contain a number of typical of terrains, including basalt flows, bajadas, ephemeral stream channels, and desert pavements. Vegetation is typical Mojave Desert scrub, dominated by creosote and blackbrush. Study plots were likewise selected at LANL to be representative of the range of backgrounds known from the area (McDonald et al. 1996, Reneau and McDonald 1996). Vegetation at this site is largely pinyon-juniper woodland (1,500-2,000 m elevation).

The size of study plots at selected study locations was determined by the FOV of the FLIR. In most cases, an area of approximately 80 cm x 70 cm was chosen. We looked for relatively vegetation-free areas where the mineral soil could been seen, and that contained a relatively high density of artifacts, either obsidian flakes or ceramics. We also selected locations where no obvious human disturbance (i.e., no tire tracks, cattle tracks, trash, etc.) was noted. The FLIR was positioned to minimize shadowing caused by the tripod, and generally a southern or western exposure was selected to maximize he amount of solar radiation on the ground surface. To capture variability in target and background materials, usually more than one study plot was imaged in any given study area. Relative abundance of artifacts, soil, and vegetation were calculated by examining digital photographs of study areas and are shown in **Table 1.**

CLNAWS Study Plots. Several study plots were selected at CLNAWS (**Figure 4a-d**). Plots were selected on substrates typical of the CLNAWS including sandy desert surfaces, rocky slopes, and colluvial pediments. Study sites were selected with the help of the CLNAWS archaeologist after touring a variety of areas on the installation. They included site 5J (so named because of its proximity to a well labeled 5J on the USGS topographic sheet), Haiwee Springs, Sugarloaf (close to one of the largest prehistoric obsidian quarries in the region), and Fossil Falls just west of CLNAWS.

Figure 2. Location map showing China Lake Naval Air Weapons Station and study plots FF-1, HS-1, SL-1, SL-2 and 5J.

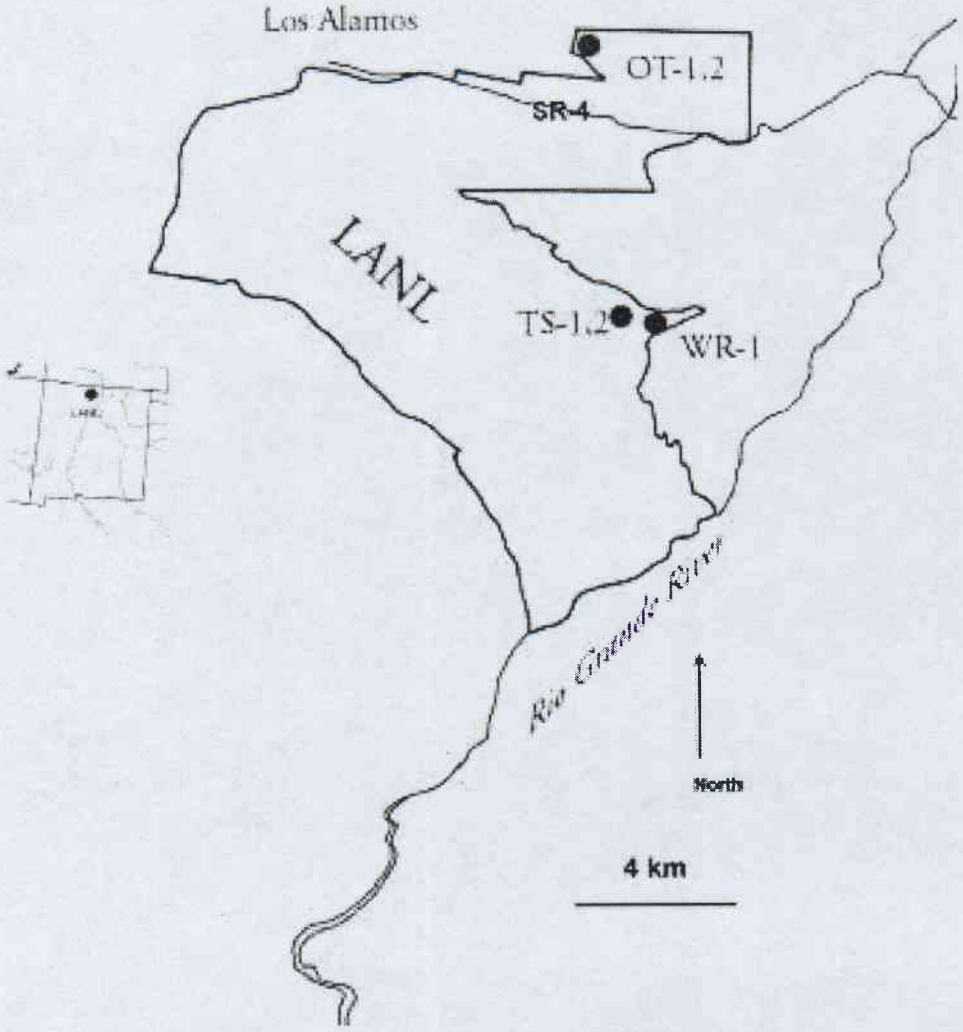

Figure 3. Location map of Los Alamos National Laboratory showing locations of study plots OT-1, OT-2, TS-1, TS-2, and WR-1.

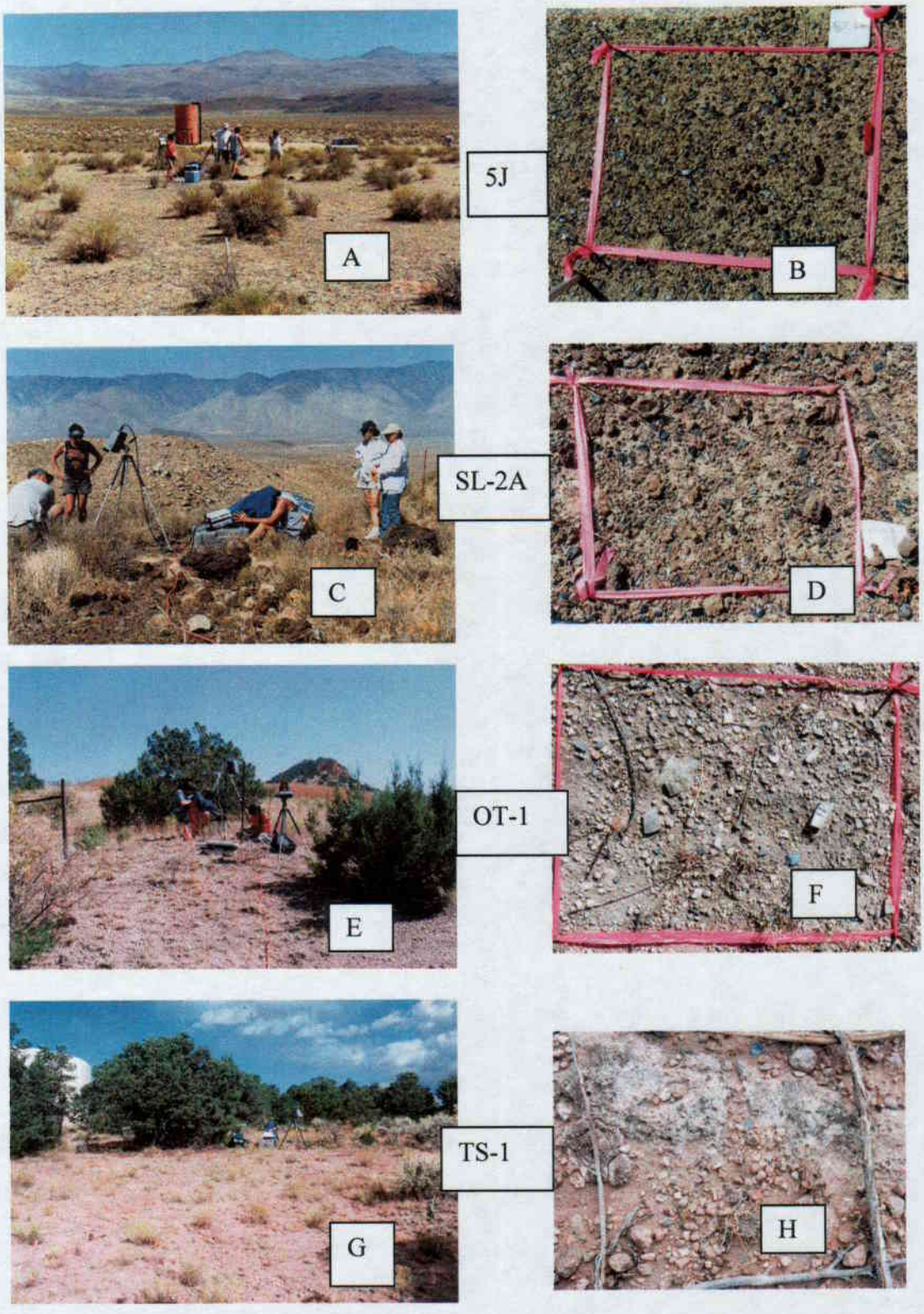

Figure 4. Selected study sites with representative study plots at China Lake Naval Air Weapons Station and Los Alamos National Laboratory. In the upper four images obsidian is the target; in the lower four ceramics are the target.

Table 1. Ground cover at study plots. Proportions of different types of artifacts were quantified for each of the study plots. Standard photographs were scanned using a HP ScanJet and manipulated in Adobe PhotoShop. By examining the standard photos and the FLIR thermal images, each artifact was identified and its area calculated. The proportion of each study plot covered by obsidian and ceramic artifacts was then calculated. This was done to provide a real-world estimate of the proportion of the ground surface covered by artifacts to keep the detection limits model realistic.

	Study plot	Dominant substrate	Percent vegetation	Percent obsidian artifacts	Percent ceramic artifacts
China Lake, California	5J-1A	Soil	<1	17	0
	5J-1B	Soil	3	14	0
	HS-1	Pebbles, soil	3.5	2	0
	SL-1	Soil, sand, pebbles, cobbles	2	6	0
	SL-2	Pebbles, cobbles	1	10	0
	FF-1	Sand, soil	<1	5	0
Los Alamos New Mexico	OT-1	Pebbles, sand	5	<1	5
	OT-2	Pebbles, soil	6	<1	6
	WR-1	Cobbles, pebbles, soil	13	<1	4
	TS-1	Cobbles, rock	3	<1	3
	TS-2	Soil, pebbles	2	<1	4

Site 5J is a an extensive scatter of obsidian tools and debitage near Coso Wash located on loose sand with grus about 30 m from the 5J well. Several plots were studied in this general area. The SW corner of Plot 5J1-A is located about 16.0 m due north of a datum marking locus 5 of the above-mentioned archaeological site. The study plot is approximately 85 cm x 70 cm in area. All the obsidian artifacts in this plot are interior flakes without cortex. No formed tools or cores were present in the study plot. Study plot 5J1B is located about 5 m northwest of 5J1A contains a somewhat lower proportion of obsidian but higher amounts of dry vegetation. Study plot HS-1A is located at Haiwee Springs archaeological site, consisting of an extensive scatter of obsidian and chert tools and associated grinding slick area. The study plot was about 60 cm x 50 cm, located on a 12-15° slope with a northeastern aspect. Basalt cobbles are abundant, and the derived soil is basaltic. Study plot SL1-A is located very near the Sugarloaf Volcanic field on a rhyolitic soil with abundant obsidian debitage. It is located about 62.0 m at a bearing of 55 degrees from USGS benchmark 14. The study plot is again about 60 cm x 50 cm, and contains two rhyolite cobbles and abundant obsidian debitage without cortex. No formed tools were seen. Study plot SL2-A is located on a vesicular basalt surface about 8.5 m at 126 degrees from USGS benchmark 14 and about 60 meters from SL1-A. This study plot contains a high proportion of vesicular basalt cobbles and gravel, and about 10% non-cortical obsidian debitage. Study plot FF-1 is located at Fossil Falls State Park just outside CLNAWS. It was selected because the archaeological site (another extensive obsidian scatter) is found on the margins of dry playa containing fine-grained sediments of the Pleistocene Owens River.

LANL Study Plots. As at CLNAWS, a variety of study plots were chosen to provide representative backgrounds **(Figure 4 e-h)**. LANL is located on the Pajarito Plateau of

New Mexico at an elevation of about 7,000 feet. At this elevation Ponderosa pine forests predominate; below is mixed pinon pine juniper woodlands. Below about 6,400 feet the now-scattered pinon juniper forests is more often dominated by sagebrush, saltbush, rabbit brush and cholla. These grow especially well on large prehistoric habitation sites. The Pajarito Plateau is composed of a series of Pleistocene ash flows and ash falls of Bandelier tuff, lying on sedimentary and volcanic rocks of middle Miocene to Pleistocene age (Purtymun and Kennedy 1971). Study sites were selected with the help of the LANL archaeologists to provide representative backgrounds with abundant artifacts. Sites included Otowi (OT), White Rock (WR), and Tshirege (TS)

Study sites OT-1 and OT-2 are located within 20 m of each other on the margins of the archaeological site of Otowi, one of the few late "magnificently large" Classic period pueblos on the Pajarito (Stuart 1989:110). It sits on the ridge which separates Pueblo Canyon from Bayo Canyon, and appears as a large somewhat lumpy hill, whose "lumps" are actually enormous rooms blocks and multiple kivas. The site itself was excavated in the early 1900's (Hewett 1904, 1909, 1953) and the room blocks are now heavily vegetated. Study plots were selected on the more-exposed slopes of the rooms blocks, where substantial densities of pottery and lithic artifacts were seen exposed on the ground surface. Both study plots are found on relatively loose friable clay-like soil weathered from the Bandelier tuff. Ceramics are the dominant artifacts consisting generally of Santa Fe black on white pottery rather than the more abundant late Rio Grande glazeware. Also present are significant amounts of dry vegetation.

Another study site was selected near White Rock, New Mexico still on the grounds of LANL. Site WR-1 is located in a sparse pinon juniper forests on tuff derived soil. The study plot is located at the margins of an archaeological site consisting of a small room block with thin trash midden. Study sites TS-1, TS-2, and TS-3 are all located on the margins of the largest village site on the Pajarito (Steen 1977:35), the ruins of Tshirege (LA-170) located about one mile north of White Rock study plots. Over 600 rooms were reported to have been present. All three study plots are located in a relatively vegetation-free areas of volcanic tuff derived soil with a roughly circular area about 8 m in diameter. TS-1 is on a slope of 1-3° with a southwestern aspect and about 30 m from the rubble mound that marks the central architectural room block of the site. This plot was located on the west side of the site. TS-2 is located about 2 m south of TS-1 in an area of loose brown sandy soil. Vegetation is very sparse, with similar slope and aspect as TS-1. Pottery and other artifacts cover about 5-10% of the surface. TS-3 is about 6 m north of TS-1 between two sagebrush.

Spectral Detection Analysis

The approach taken to determine target detectability is referred to as "spectral detection analysis" (Sabol et al. 1992). This method is designed to evaluate the spectral contrast between the target and background materials to determine detection thresholds. Initially, laboratory (or high-resolution field) spectra are convolved to the bands of a selected imaging system (TM, AVIRIS, FLIR, TIMS, ASTER, and SEBASS in this study) (**Table 2**). To account for target spectral variability, the mean and standard deviation spectra of the targets were used in the analysis. Detection thresholds were

determined for both obsidian and pottery against background mixtures of soil/vegetation, basalt/vegetation, and granite/vegetation using spectral mixture analysis.

Table 2. Band characteristics of imaging systems used in this study.

	System	Bands	Wavelengths (μm)
VIS/NIR	TM	6	0.45 - 0.52 0.52 - 0.60 0.63 - 0.69 0.76 - 0.90 1.55 - 1.75 2.08 - 2.35
	AVIRIS	224	Bands evenly spaced 0.38 - 2.50 μm
THERMAL	FLIR(a)	3	8.22 8.66 11.73
	FLIR(b)	3	8.51 9.11 10.80
	ASTER	5	8.20 - 8.40 8.60 - 8.80 8.90 - 9.20 10.30 - 10.90 10.90 - 11.50
	SEBASS	128	Bands evenly spaced 7.50 - 13.50 μm

The occurrence of multiple components in a scene at the sub-pixel scale results in mixed spectra in an image. The fractions of the components can be determined from the mixed spectrum if the component spectra are known using "spectral mixture analysis." A linear mixing model is used to describe the case where the surface components are large and/or opaque enough to allow photons to interact with only one component (Adams and McCord 1971; Nash and Conel 1974; Singer and McCord 1979). Mathematically, linear mixing comprises linear combinations of component (endmember) spectra:

$$DN_b = \sum_{em=1}^{Ne} F_{em} DN_{em,b} \quad ; \quad \sum_{em=1}^{Ne} F_{em} = 1$$

where, DN_b is the radiance for each channel (b), *Ne* is the number of spectral endmembers (components in the scene), and F_{em} is the fraction of endmember *em*. The sum of the fractions of the endmembers equals 1 (100%).

In spectral unmixing, this equation is inverted using least-squares regression while constraining the fractions to sum to one. For a given number of spectral components in

the model (*ne*) and bands (*b*), this has the same effect as simultaneously solving for *ne* fractions from a set of *b* equations. The above equation can be rewritten and modified as:

$$DN_b = ((EM_{1b} F_{1b}) + (EM_{2b} F_{2b}) + (EM_{3b} F_{3b}) F_{em} + ..(EM_{ne_b} F_{ne_b})) + E_b + noise_b$$

$$\text{and} \qquad \sum_{em=1}^{ne} F_{em} = 1$$

where DN_b is the reflectance of the linear mixture of the components $EM1_b$ to $EMne_b$ present in respective fractions of $F1_b$ to Fne_b, and $noise_b$ (instrumental noise). A high signal-to-noise (>200/1), common in current imaging systems, was assumed in this study. E_b, the residual signal, this that part of the measured spectrum that is not modeled as a mixture of the endmembers or as noise. When mixing spectra, there are no limits on then number of bands. However, when unmixing a spectrum, the number of components (*ne*) must be less than or equal to the number of bands (*b*), leaving at least one degree of freedom to determine the root-mean-square (*rms*) fit. The *rms* is the combination of the E_b term over all image channels (*M*).

$$rms = (M^{-1} \sum_{b=1}^{M} E_b^2)^{.5}$$

To characterize the spectral variability of both obsidian and pottery, the following spectra (for each obsidian and pottery) were derived from the multiple samples collected: 1) a mean spectrum, 2) a mean plus one standard deviation spectrum, and 3) a mean minus one standard deviation spectrum. Background and target materials were mixed, at a range of proportions, combined with different samples of noise, and unmixed to estimate the fractions of the target materials. The resulting spread of fractions about the initial proportions of the mixture was due to target variability and noise. This distribution, assumed to be gaussian, can be contoured into confidence intervals; from which detection thresholds were determined.

Detection Modeling Results

Visible/Near-infrared

The detection thresholds for pottery and obsidian were found to be high, greater than 85% (85% being the best case in our simulated experiment) for both TM and AVIRIS bands. As previously stated, the detection of a target is dependent upon the spectral contrast between the target and mixtures of the background. In this study, we found that pottery and obsidian are spectrally similar to common backgrounds, reducing their detectability in the visible to near-infrared. This can be seen in **Figure 5** where various pottery spectra are shown by the mean (heavy black dashed line) and standard deviation (dark gray). The spectral shapes of the pottery mimic mixtures of shade and soil.

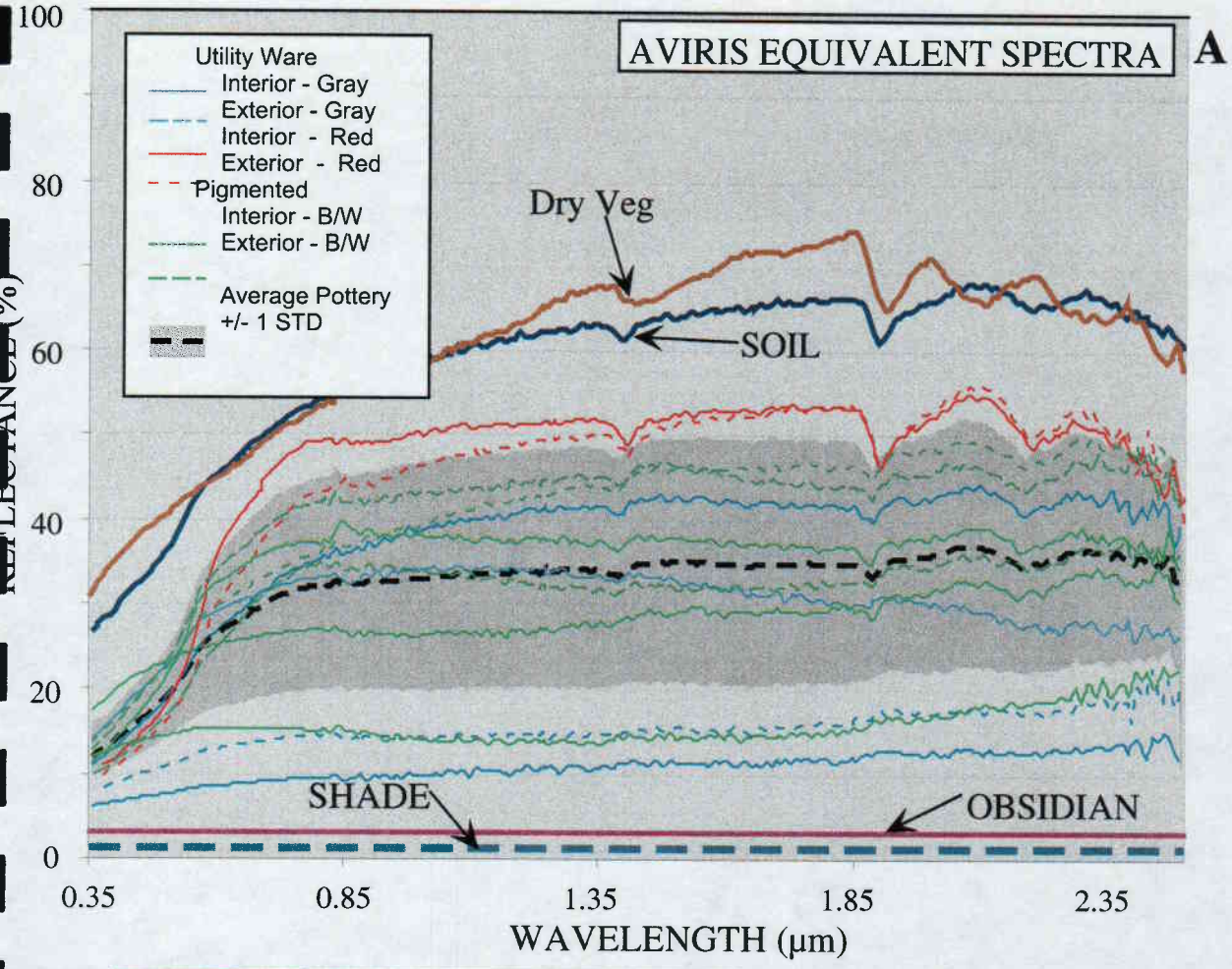

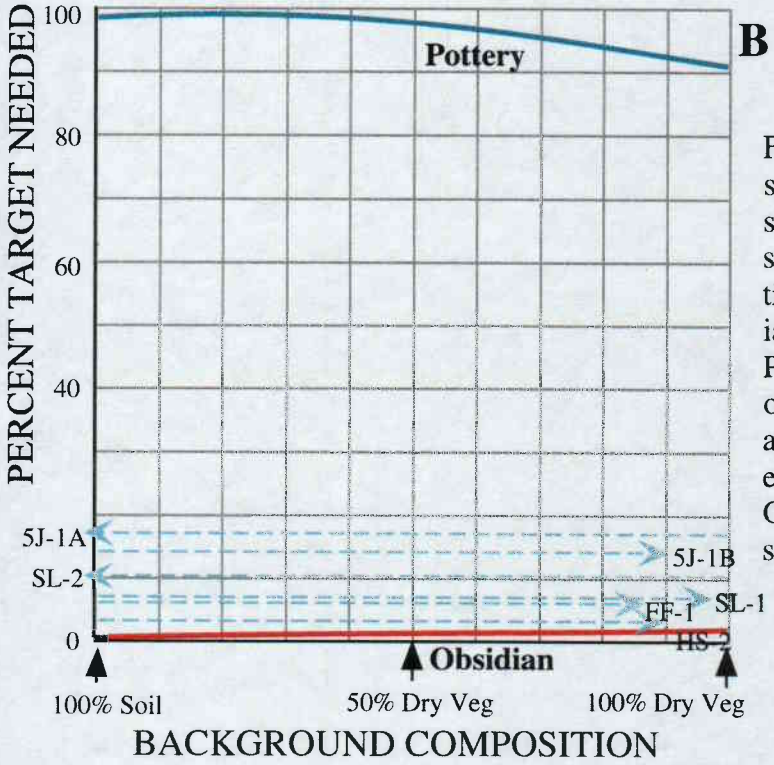

Figure 5: A) Pottery and background spectra. The mean pottery spectrum is shown as a black dashed line with the standard deviation in gray. B) Detectiion thresholds for pottery and obsidian artifacts using AVIRIS bands. Pottery is virtually undetectable. The obsidian detection curve is only appropriate if shade from other sources can be eliminated (see text). Otherwise, obsidian is too spectrally similar to shade to be detected.

Additionally, some granite spectra are nearly identical to the brighter pottery spectra (not shown).

The spectra of obsidian is a flat 4% reflectance in the visible/near-infrared. These spectra closely resemble the spectra of shadows, especially in the presence of noise. Obsidian cannot be effectively detected unless shade (topographic shading and shadows as well as unresolved shadows cast by vegetation) can be removed prior to image modeling. This is, most likely, possible only under ideal conditions (flat or gentle relief, smooth surface, minimal vegetation). Under these unique circumstances, obsidian is detectable at fractions of 2 to 3%.

The detection thresholds for pottery and obsidian artifacts are shown on the bottom of **Figure 5** AVIRIS equivalent spectra. This graph shows the "percent of target needed" to be detectable (vertical axis) against different "background compositions" (horizontal axis). The curves indicate the minimum fraction of target (pottery or obsidian) required to be detected against backgrounds composed of: 1) soil and vegetation (in red), 2) granite and vegetation (in black), and 3) basalt and vegetation (in dark purple). The detectability depends on the fractional composition of the background and, therefore, is plotted as a curve. In short, the lower the detection threshold, the higher the detectability. Dashed lines at the bottom of each detection threshold graph are the fraction of artifact found at various sites. These fractions were determined from both FLIR images and photographs (at a 0.6-0.7 meter scale) and are detailed in **Table 2**. Using this analysis of individual spectra, artifacts are detectable when a detection threshold curve falls below the dotted line for a particular site.

Thermal Infrared

The detection thresholds for pottery and obsidian artifacts, depicted for different thermal imaging systems in **Figures 6 through 10**, are all in the same format. On the left side of the figure are the detection thresholds similar to that described above. On the right side of each figure is a spectral plot of components used to determine the thresholds. Numerous artifact spectra were used to establish pottery and obsidian variability. Their means are shown as a dotted line with one standard deviation in gray.

Laboratory, 2μm – 15μm. The JPL laboratory thermal spectrometer measures 2257 bands between 2.0 and 15.0 μm. Artifact detection thresholds at this spectral range are shown in **Figure 6**. Pottery thresholds are lowest (highest detectability) against granite/vegetation backgrounds, with a minimum of 37% pottery needed to be detected against a "pure" granite background and a maximum of 72% needed against "pure" vegetation. All of these thresholds are significantly higher than the fraction of pottery observed in the field at LANL (maximum of 6%). Obsidian thresholds range from 8% ("pure" granite background) to 20% (50% vegetation / 50% basalt background) and would be

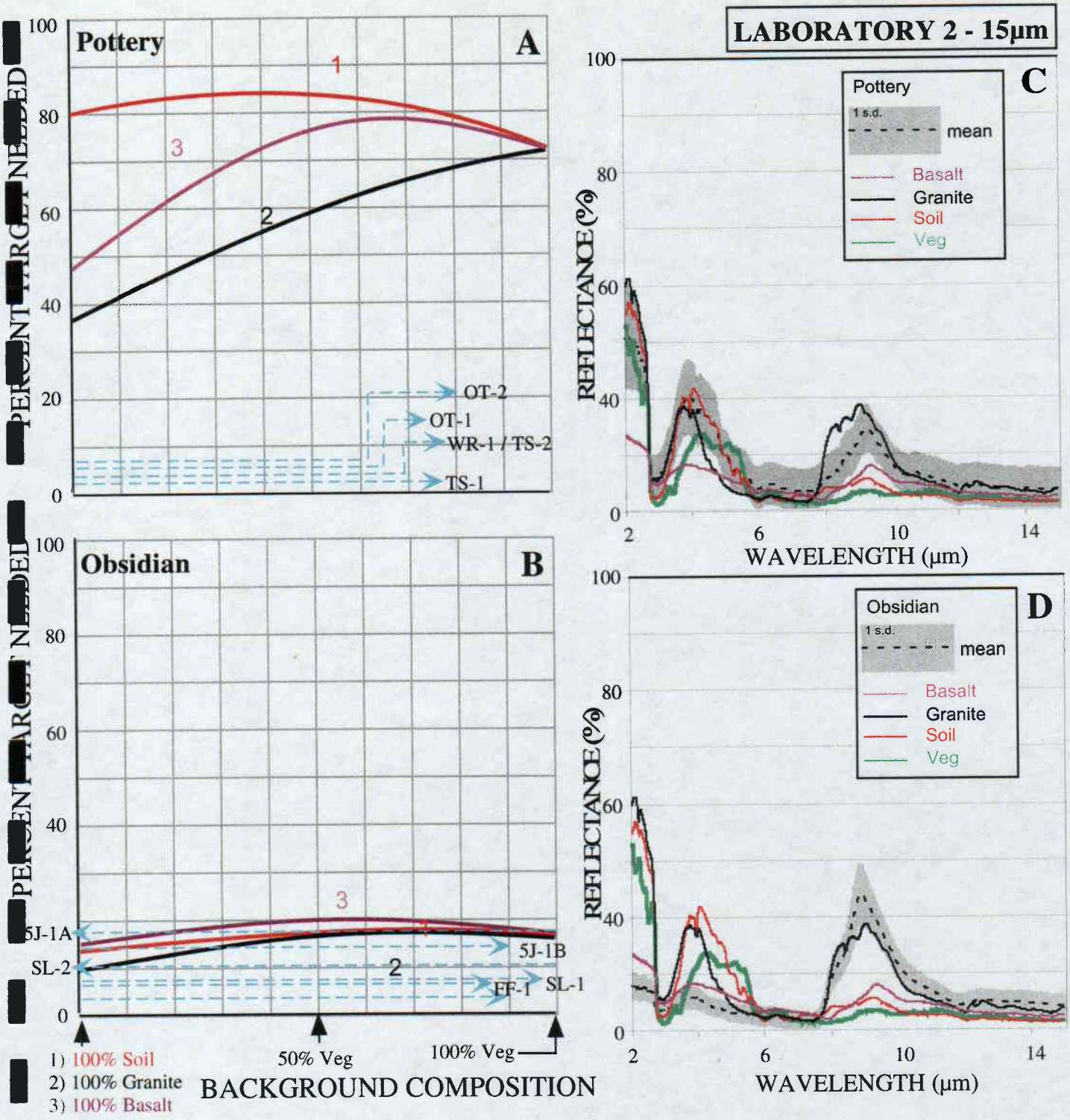

Figure 6: Detection thresholds for pottery sherds (A) and obsidian artifacts (B) using the full range of laboratory spectra (2 - 15µm). The results for each substrate background (in mixtures with vegetation) are shown as: 1) soil (red), 2) granite (black), and 3) basalt (purple). The spectra used in the analysis are shown in C (pottery and backgrounds) and D (obsidian and backgrounds). The mean sprectrum for the artifacts is shown as a black dashed line with the standard deviation in gray.

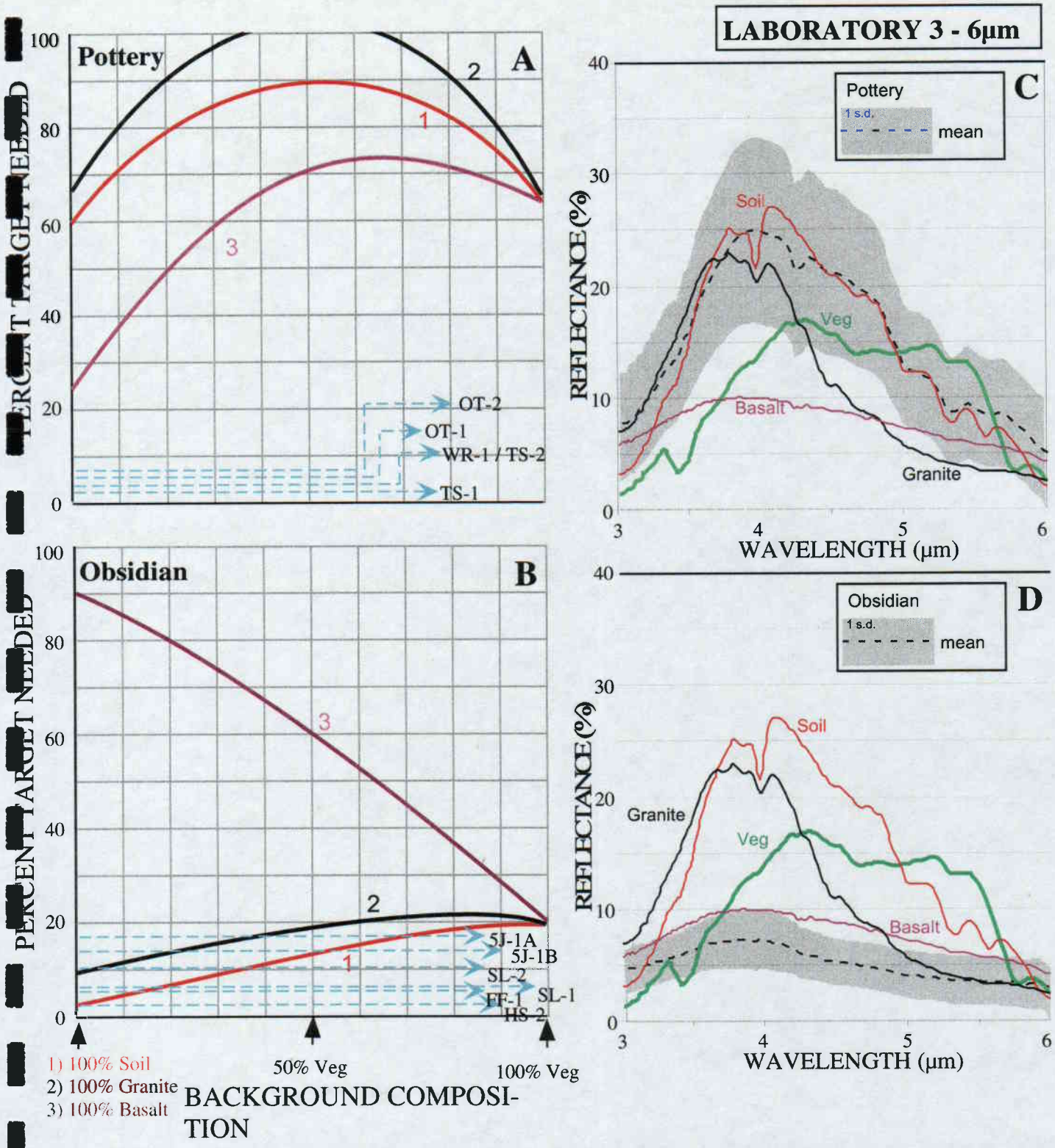

Figure 7: Detection thresholds for pottery sherds (A) and obsidian artifacts (B) using laboratory spectra (3 - 6µm). The results for each substrate background (in mixtures with vegetation) are shown as: 1) soil (red), 2) granite (black), and 3) basalt (purple). The spectra used in the analysis are shown in C (pottery and backgrounds) and D (obsidian and backgrounds).

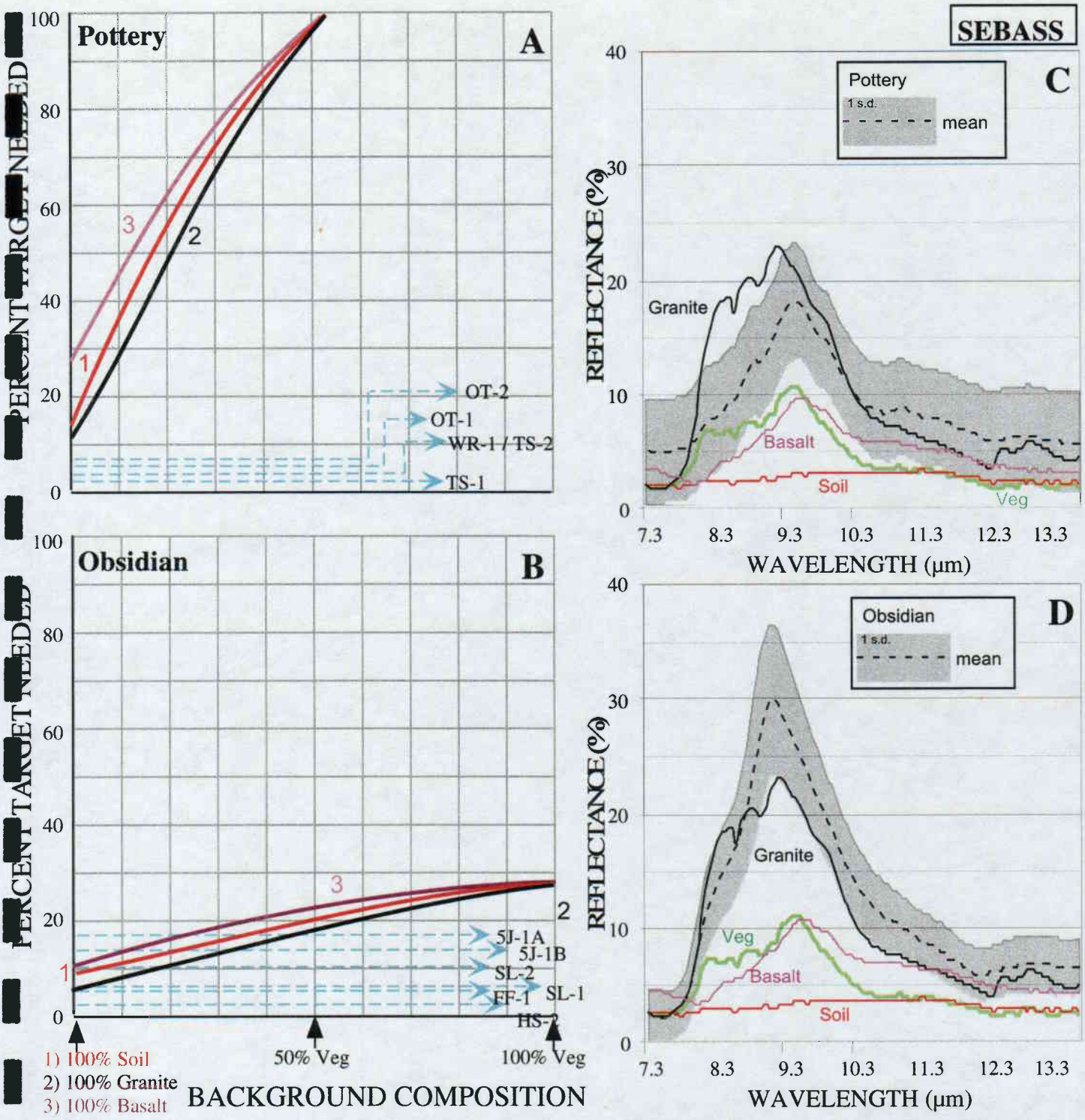

Figure 8: Detection thresholds for pottery sherds (A) and obsidian artifacts (B) using SEBASS bands. The results for each substrate background (in mixtures with vegetation) are shown as: 1) soil (red), 2) granite (black), and 3) basalt (purple). The spectra used in the analysis are shown in C (pottery and backgrounds) and D (obsidian and backgrounds). The mean sprectrum for the artifacts is shown as a black dashed line with the standard deviation in gray.

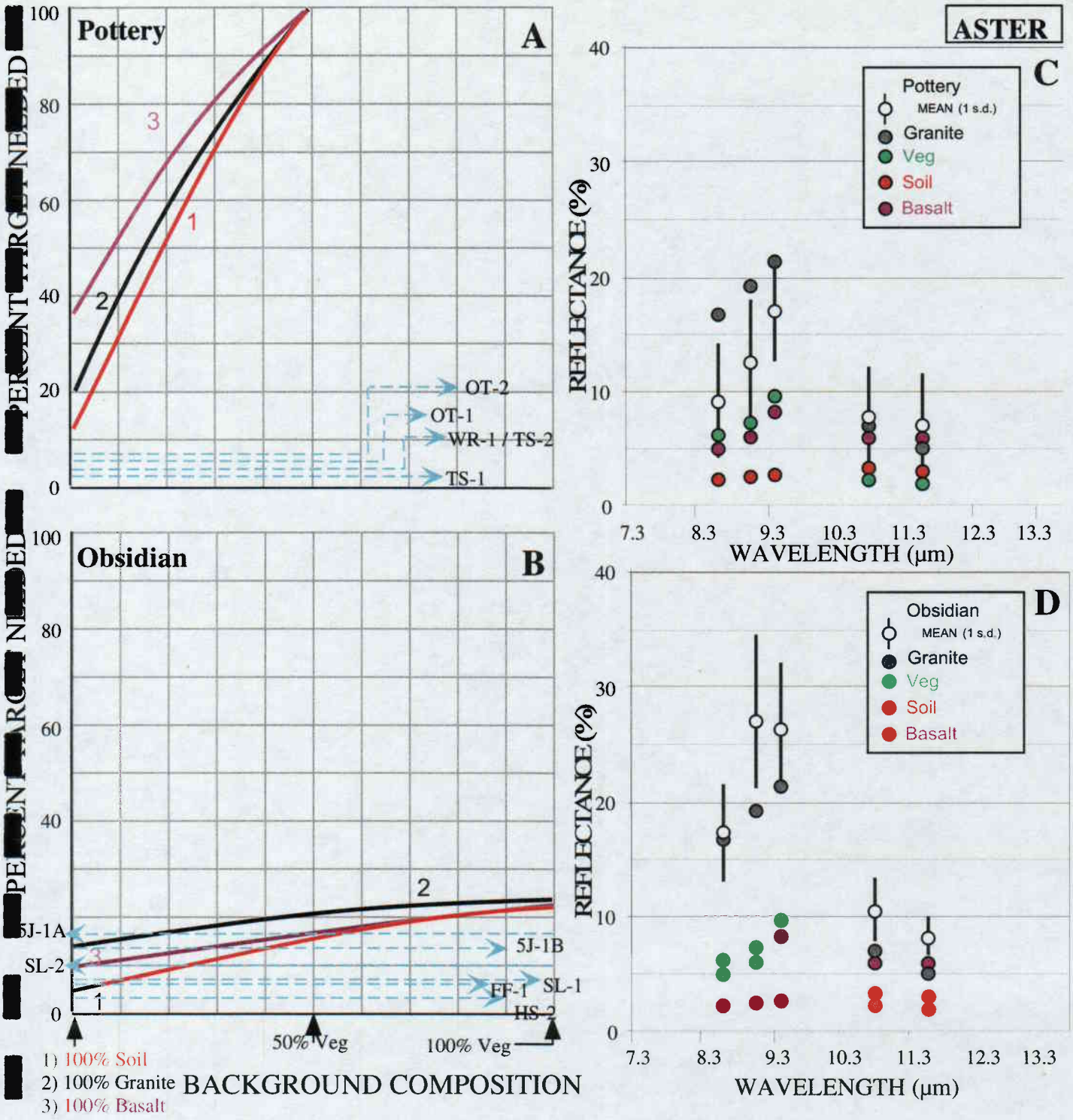

Figure 9: Detection thresholds for pottery sherds (A) and obsidian artifacts (B) using ASTER bands. The results for each substrate background (in mixtures with vegetation) are shown as: 1) soil (red), 2) granite (black), and 3) basalt (purple). The spectra used in the analysis are shown in C (pottery and backgrounds) and D (obsidian and backgrounds). The mean sprectrum for the artifacts is shown as a white circle with the standard deviation as a vertical bar.

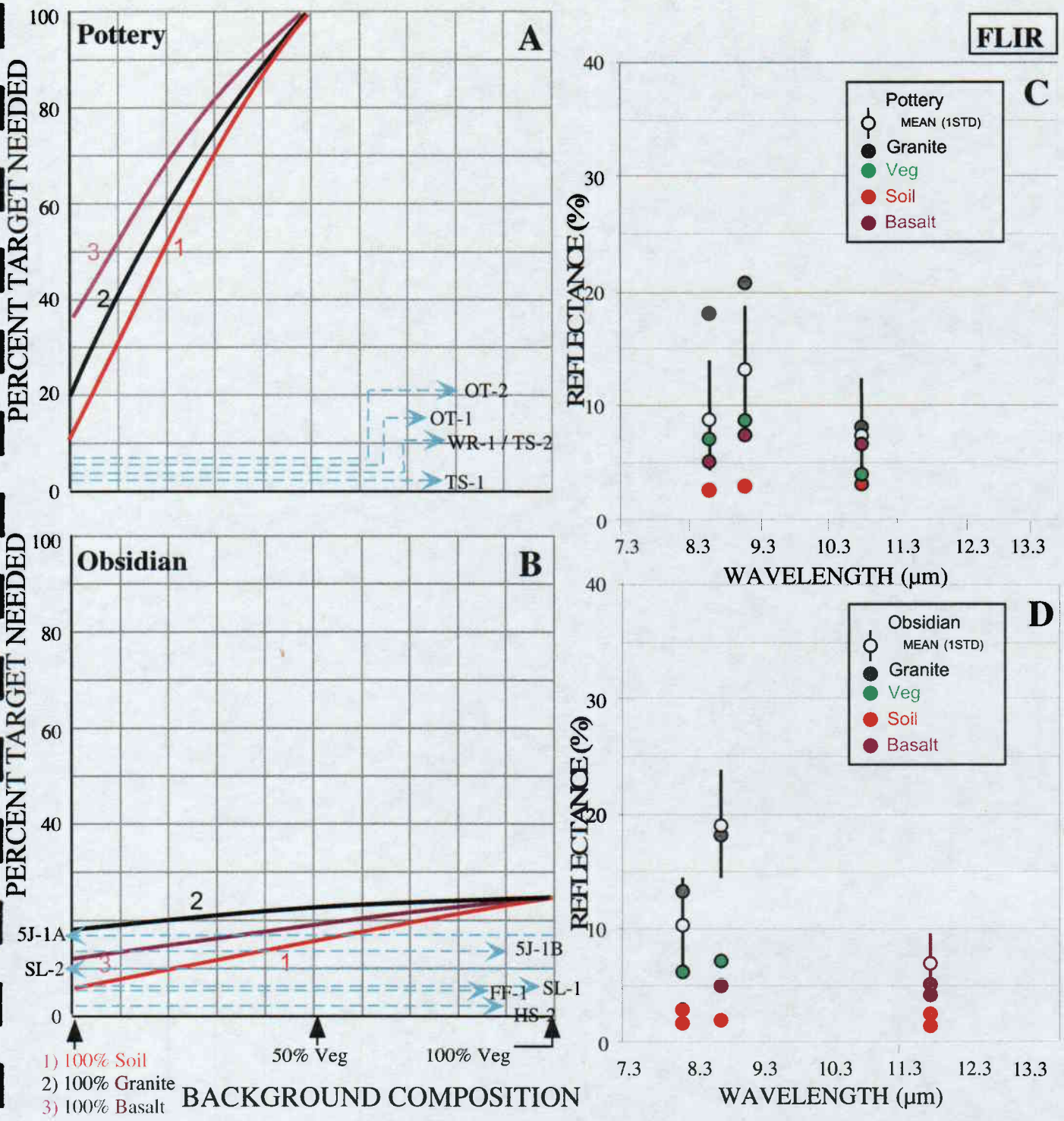

Figure 10: Detection thresholds for pottery sherds (A) and obsidian artifacts (B) using FLIR bands. FLIRa bands were used for the obsidian while FLIR b were used for the pottery. The results for each substrate background (in mixtures with vegetation) are shown as: 1) soil (red), 2) granite (black), and 3) basalt (purple). The spectra used in the analysis are shown in C (pottery and backgrounds) and D (obsidian and backgrounds). The mean sprectrum for the artifacts is shown as a white circle with the standard deviation as a vertical bar.

detectable in half of the study sites at CLNAWS. This improved detection is due to the greater spectral contrast between obsidian and backgrounds between 3-6μm and between 8-11μm).

Laboratory, 3μm – 6μm. A sub-sample of the full thermal laboratory spectra (above) were used to evaluate detectability at the 3-6 μm range of the spectrum. Normally, this spectral range is ineffective in remote sensing due to the broad water absorption feature at 3μm. Water in the atmosphere absorbs thermal energy at these wavelengths before being received by satellites or high-flying aircraft. However, measurements made on the ground (or in low-flying aircraft) in dry climates (deserts) minimize this effect, making these data potentially useful. Pottery thresholds (**Figure 7**) remained high against backgrounds of vegetation and soil/granite (>60%). However, they decreased to as low as 25% against basalt/vegetation. Obsidian thresholds improved to 2-3% (soil). Basalt, which is spectrally similar to obsidian at these wavelengths had very low detectabilities under conditions of low vegetation (80-90% threshold).

SEBASS. The Spatially Enhanced Broadband Array Spectrograph System (SEBASS) is a high resolution thermal imaging system built by the Aerospace Corporation. It has 128 bands between 7.5μm and 13.5μm, a spectral region sensitive to surface silica content. Pottery thresholds ranged from 12%, 15%, and 28% for "pure" granite, soil, and basalt, respectively. Pottery is undetectable in backgrounds containing >50% vegetation. Obsidian thresholds remained low (5%, 9%, 10% for "pure" granite, soil, and basalt) and would be detectable in most of the field study sites **(Figure 8)**. Granite substrates yield the lower detection thresholds even though the spectral contrast between granite and the artifacts appears to be less than other substrates. This is primarily due to the unique spectral signature of granite, which, during unmixing, reduces uncertainties caused by background mixtures mimicking targets.

ASTER. ASTER (Advanced Spaceborne Thermal Emission Reflection Radiometer) is a thermal imaging system on the TERRA satellite launched into Earth orbit in January 2000. ASTER images will be begin to be available in Spring 2000. Pottery and obsidian thresholds **(Figure 9)** were slightly higher than those found using SEBASS bands. Thresholds for pottery are lowest for "pure" substrates of granite (12%), soil (20%), and basalt (37%) and rise to ~100% when vegetation cover exceeds 50%. Obsidian thresholds with backgrounds of "pure" soil, basalt, and granite were 4%, 10%, and 15% respectively.

FLIR. The FLIR (Forward Looking Infrared Radiometer) is an imaging system built by FLIR Systems Incorporated (FSI) in Beaverton, Oregon. The Geological Sciences Remote Sensing Laboratory at the University of Washington has modified this system to image three spectral bands and uses it as a field instrument. This system was taken into the field to image several sites in each study area **(Table 1)**. After the field visit to CLNAWS, but prior to the LANL trip, the FLIR filters were changed to be more similar to three of the ASTER bands. Hence, the filters used for detecting obsidian at CLNAWS are referred to as FLIRa and those used for pottery sherds at LANL are FLIRb.

Obsidian thresholds (FLIRa) **(Figure 10)**, similar to those determined from ASTER bands, were below that required to be detected in the FLIR images taken of CLNAWS

study plots. A typical FLIR image, along with a corresponding photograph are shown in **Figure 11** (obsidian near Sugarloaf Mountain, CA). The detection threshold for obsidian in this scene was determined to be 5%. In fact, twice this amount (10%) occurs in the image. Hence, obsidian should be detectable in images of this area at the 0.6-0.7 meter pixel scale using FLIRa bands.

Pottery thresholds, like the obsidian thresholds, are similar to those of ASTER. They range from 12% for "pure" soil to being undetectable with over 48% vegetation with the substrate. A typical FLIR image and photograph is shown in **Figure 12** (pottery sherds at the Otowi ruins, LANL). The threshold for this area is 18%, far more than the 5% at this particular site.

Discussion/Conclusions

Detection of Artifacts

The visible/near-infrared spectrum does not appear to be useful for detecting pottery, and may only be useful for obsidian if shade can be removed independent of the obsidian. Topographic shade removal requires the use of a digital elevation map (DEM). The scale of current (and most available and commonly used) U.S. Geological Survey 7.5' DEMs, allows for removal of only coarse estimates of topographic shading. It does not account for the sub-pixel topography caused by vegetation, rocks, boulders, and small-scale landform variations. This approach may work if: 1) the surface is generally flat or gradually variable, 2) unvegetated, and either a) pebbles and rocks lie flat on the surface, or b) the image is taken when both the sun and imaging camera are directly overhead.

The thermal portion of the spectrum, being sensitive to the silica content of the surface, is much more conducive for pottery and obsidian detection. Pottery detectability is its greatest against mineral substrates (soil, granite, and basalt) and typically degrades with the addition of vegetation. Pottery was most detectable against substrates using SEBASS wavelengths (a minimum of 12%). The full range thermal laboratory spectrum (2-15μm) as well as the 3-6μm laboratory indicates the potential to detect pottery against vegetation when the pottery fraction is high (>67%). The high spectral resolution of laboratory and SEBASS spectra better define the spectral shape of the components, thereby minimizing spectral mimicking during unmixing. The few bands of the ASTER and FLIR systems increase the potential for this mimicking problem.

The study plots on LANL contained low fractions of pottery (6% maximum) and would not be expected to be detectable using the thermal imaging systems. However, some sites in the southwestern U.S. such as Pottery Mound near Albuquerque and in portions of the Old World such as ancient Egypt (**Figure 13**) contain far greater proportions of the ground surface covered with pottery. It is possible that current imaging systems could detect pottery in these sites.

The potential for thermal imaging to detect obsidian is excellent. Detection thresholds were low; between 4% and 14% against "pure" substrate. The FLIR image in

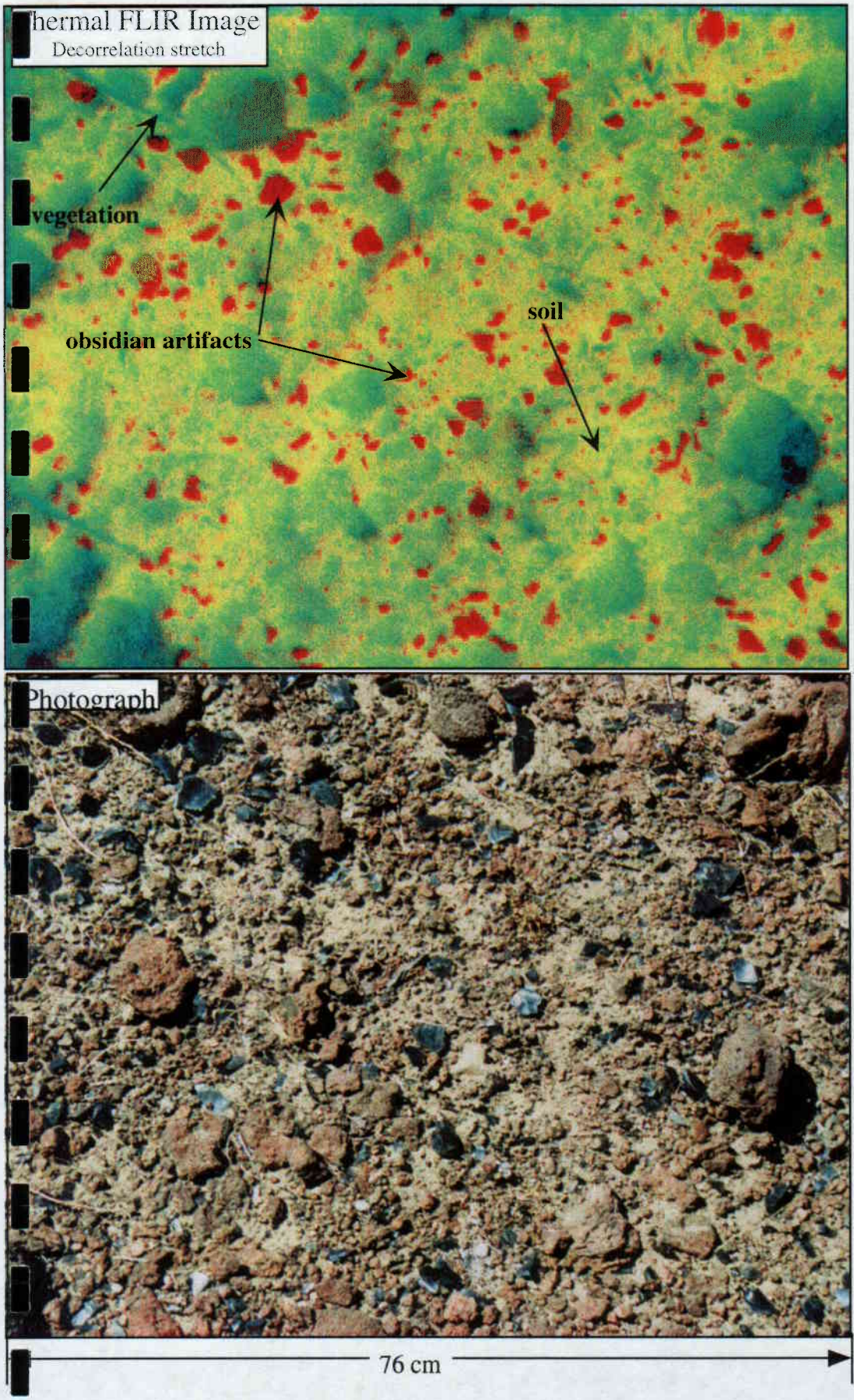

Figure 11: FLIR thermal image and photograph of site SL-2 near Sugarloaf Mountain (China Lake area, CA). The images were taken on 23 July 1999 at 9:45am and contain 10% obsidian, 1% vegetation, and 89% substrate. FLIRa bands were used.

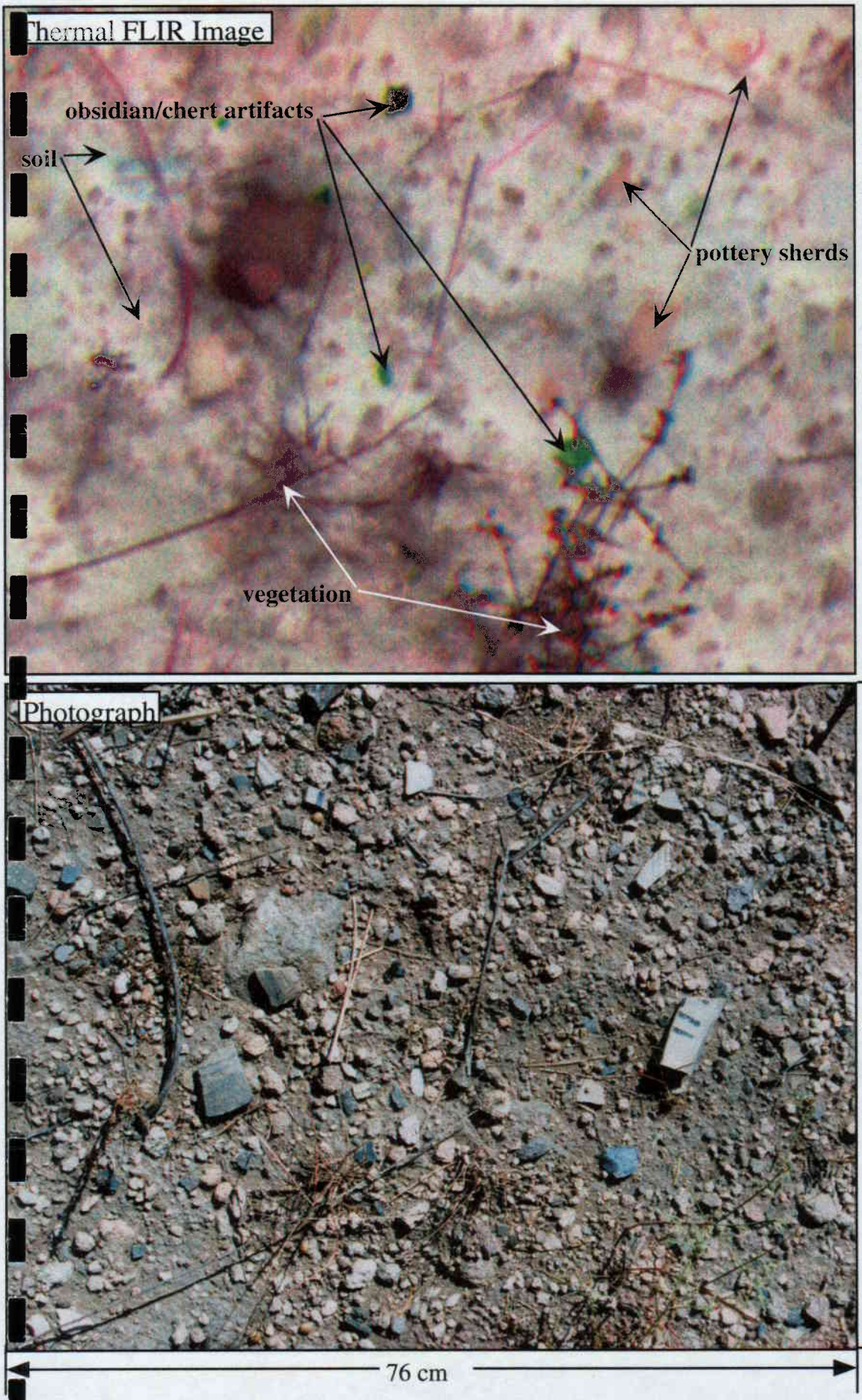

Figure 12: FLIR thermal image and photograph of site OT-1 in the Otowi ruins near Los Alamos, NM. The images were taken on 5 October 1999 at 1:00pm and contain 5% pottery sherds, <1% obsidian/chert chips, 5% vegetation, and 89% substrate. FLIRb bands were used.

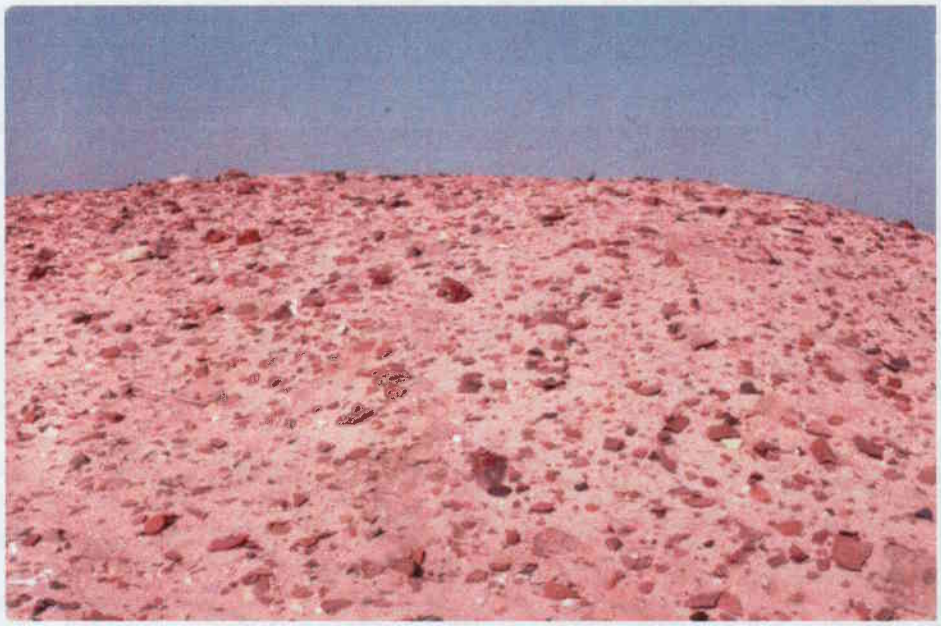

Figure 13. Photograph of dense ceramic scatter at the ancient Roman site of Tebtunis, near Cairo, Egypt.

Figure 11 shows how clearly obsidian stands out in the thermal as compared to the visible spectral region.

Spatial scale

Our study was designed to specifically evaluate the spectral detectability of artifacts in mixtures with backgrounds (a single spectrum). Another, equally important factor in target detection is the spatial aspect. The spatial distribution of a target in an image may increase its chances for detection. For example, say that a target material occurs over an area that, in an image, is represented by several pixels. Even if the occurrence of the target is below the detection threshold (based on analyzing a single mixed spectrum), it may be detected as a coherent group of pixels with similar sub-threshold target fractions. The drawing in **Figure 14** illustrates the importance of incorporating spatial patterns in conjunction with spectral attributes to detect targets. An image containing no target appears with low levels of random noise (**Figure 14a**). All fractions are below target thresholds. The same image containing three multi-pixel clumps of low fractions of target material appear as spatially distinct areas indicating the presence of the target material **(Figure 14b).**

Because the FLIR is an imaging system, we were able to evaluate the spatial distribution of artifacts on the 0.6-0.7 meter scale. Using FLIR images and site photographs, we produced a 1024 pixel by 1024 pixel image showing the area covered by typical distribution and size of obsidian artifacts over a one square meter area. In this image, areas that contained 100% target were coded as 100 and areas on only background were coded as 0. The original 1024 by 1024 image contained 11% obsidian and 89% substrate. We then degraded the image by averaging over 2, 4, 8, 16, 32, 64, 128, 256, 512, and 1024 pixels. Then, assuming a detection threshold of 10%, we highlighted (in white) all of the image pixels containing detectable obsidian. The images and a plot of the resulting changes in the fraction of detectable target are shown in **Figure 15**. The averaging resulted in mixed pixels around the obsidian artifacts. As the pixel size increases, the effect of the mixing spreads; such that the percent of detectable obsidian in the original 1024^2 image (11%) increases to 100% in the single pixel image. Increasing the detection thresholds to 15% and 20% shows a peak in the area covered with detectable target when the image was degraded to 64 by 64 pixels and a subsequent drop as the pixel size increases such that there is no detectable target in the 4 by 4 pixel image.

Images typically have pixel sizes in the tens of meters. The same effect caused by mixing continues at scales greater than a meter. We designed a theoretical example to demonstrate this effect. Typical archaeological sites have a small area (5m x 5 m) with a high fraction of target material surrounded by progressively lower densities of artifacts. The size of archaeological sites is highly variable. However, for this test we defined sites as covering 25 m x 25 m with a central area (5 m x 5 m) composed of 17% target. Immediately surrounding this central is a 5 meter buffer of 5% target, around which is another buffer of 1% target (**Figure 16A**). Sites were spaced approximately 100 meters apart in a one kilometer image. Similar to the example shown in Figure 10, this 1024 by 1024 image was degraded and the percent of detectable target in the image plotted relative to pixel size (**Figure 16B**). Curves for detection thresholds of 2% and 5% were

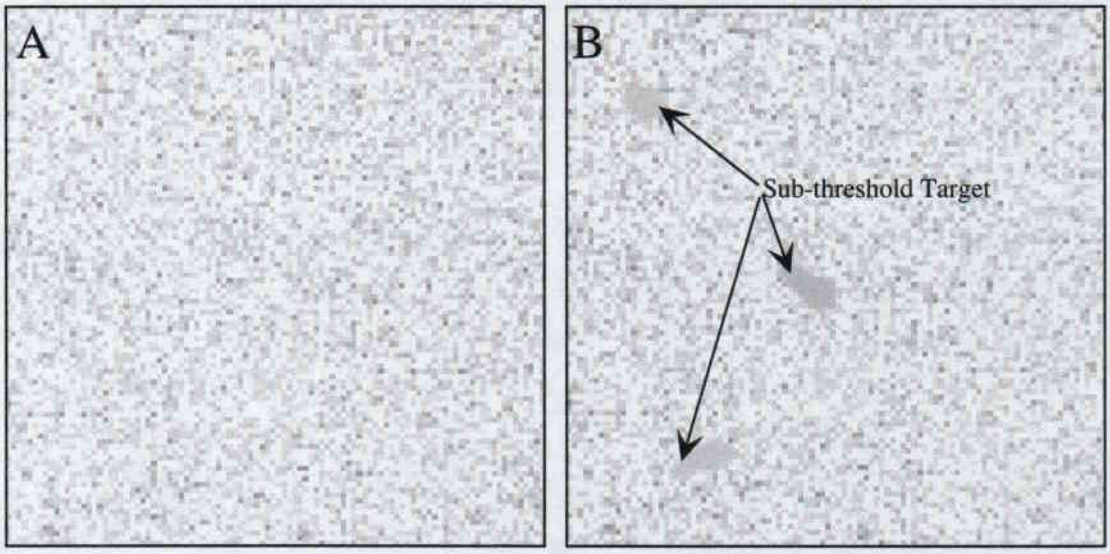

Figure 14: A) Image containing no target material (only background). Only low levels of random noise showing sub-threshold target fractions. B) The same image which now contains three multi-pixel groups of sub-threshold target.

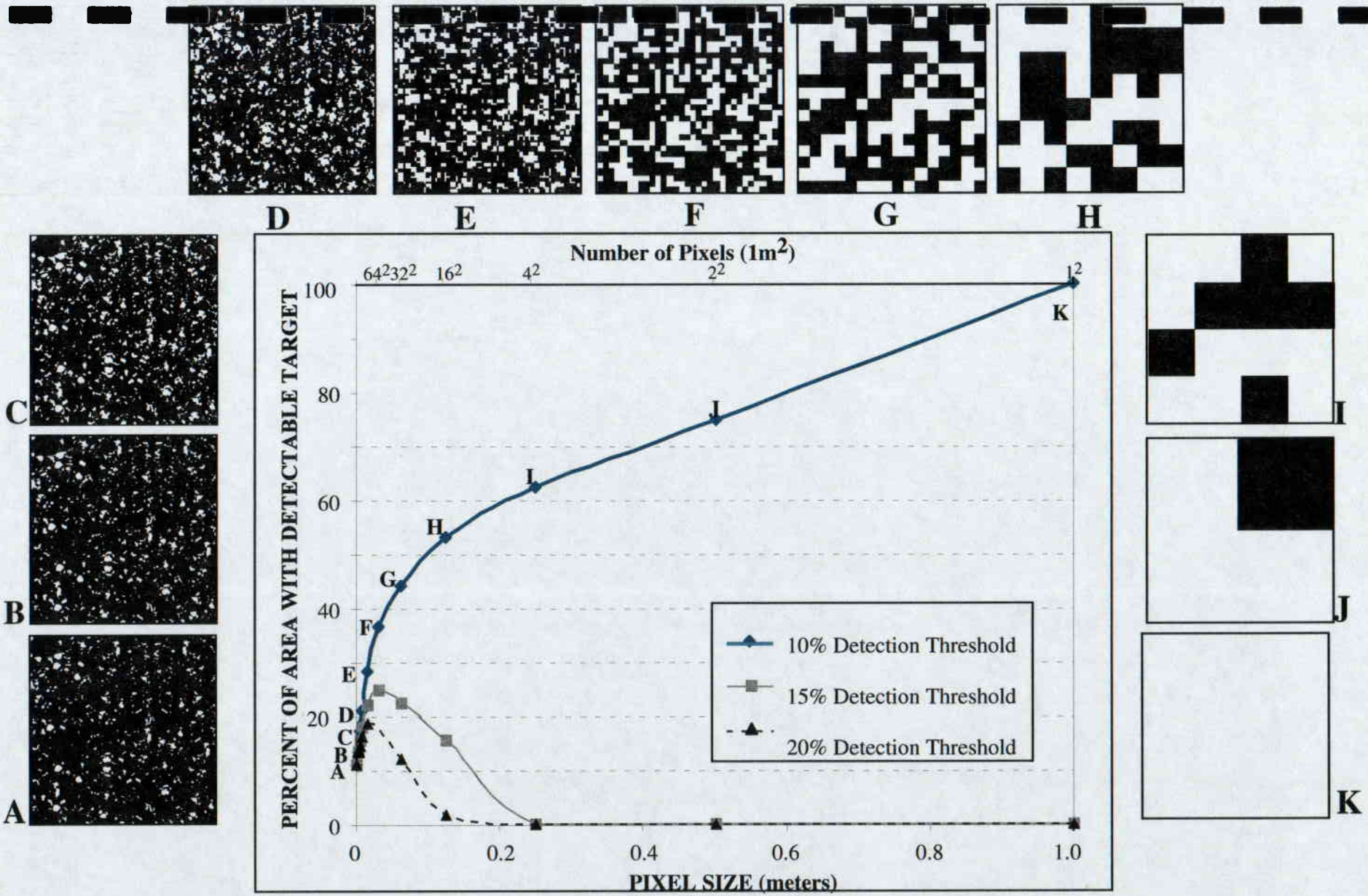

Figure 15: Graph of the change in detectable target (up to a 1 meter scale) as a result of change in pixel size at 10%, 15%, and 20% detection thresholds (see text). The images labeled A thru K pertain only to the 10% detection threshold.

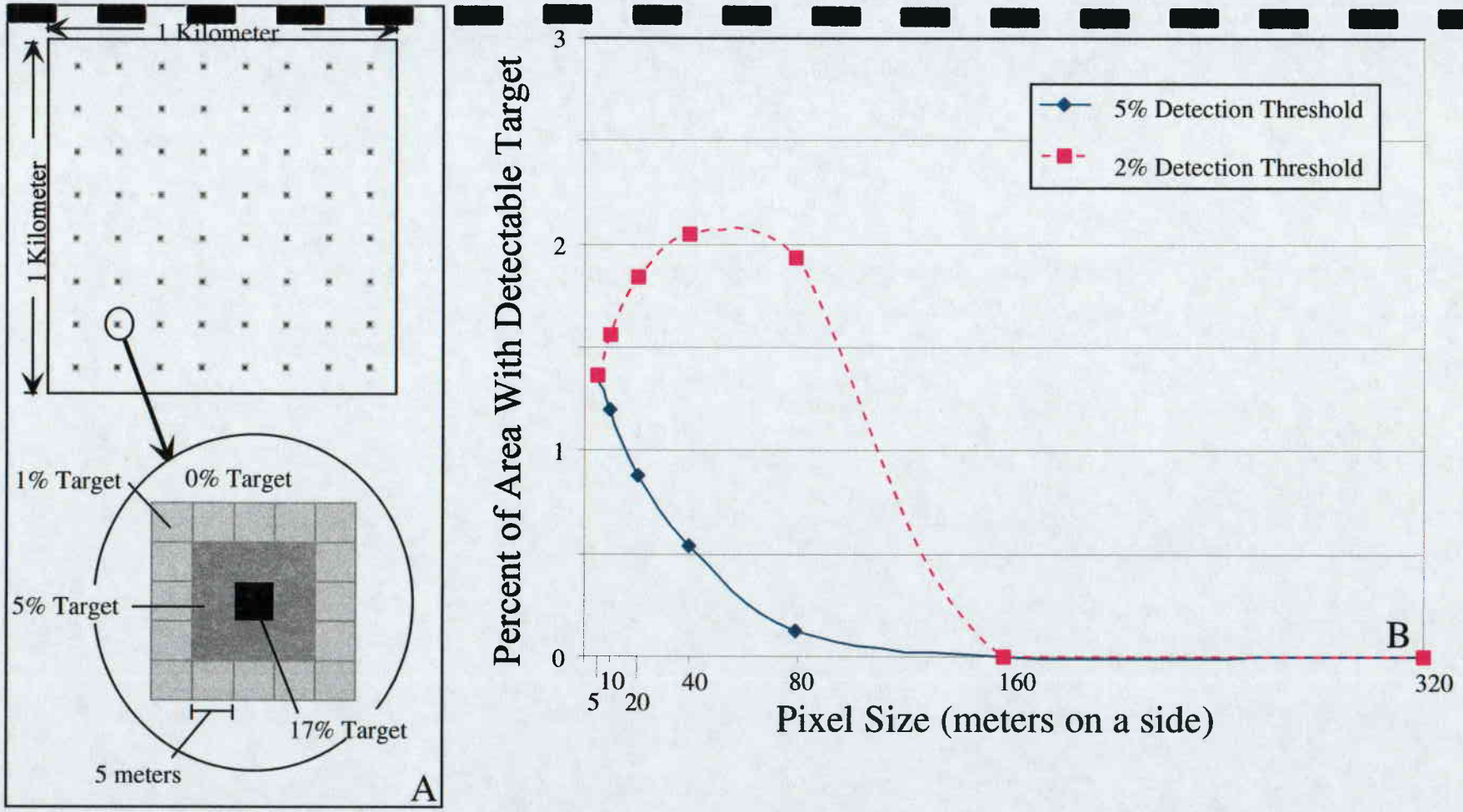

Figure 16: Change in area with detectable target as a result of change in pixel size from 1 meter to 1 kilometer. A) The experimental image setup for this text (see text). B) Curves showing theat 2% and 5% detection thresholds.

determined. The examples shown in **Figures 15 and 16** are simple demonstrations of the role of spatial analysis in detection theory in very specific cases . They demonstrate the factors that determine the optimal pixel size when detecting sub-pixel in images: 1) target size and distribution, 2) pixel size, and 3) the detection threshold (which depends upon the spectral contrast between target and background).

Temporal Analysis

Another approach not addressed in this study is the differential rates of heating and cooling of different surface materials. Specifically, the differences in materials between midday (when the surface is its warmest) and late at night (at its coolest), can be used to identify and map targets. An example of the differential heating/cooling of obsidian and background soil over an 18-hour period (as measured in the field using the FLIR) is shown in **Figure 17**. In the morning, both obsidian and soil warm at similar rates. However, at midday, the relative radiance of obsidian is significantly less than that of the soil. This same measurement was not performed on pottery due to the poor weather conditions in the field (in New Mexico). However, we expect that the denser pottery sherds would tend to heat and cool at different rates than the less-dense background soil; making this approach potentially useful for pottery detection.

Summary of Conclusions

- In the visible/near-infrared, pottery mimics mixtures of shade and substrates (rocks and soils), making it undetectable. Obsidian mimics shade, and therefore, can only be detected is the effects due to shading are removed through topographic modeling where vegetation is scarce.
- The thermal infrared portion of the spectrum is more useful for detecting obsidian and pottery artifacts than the visible/near-infrared. Pottery may be detectable in the thermal, but only at high percent surface coverage (~<20%) and under minimal vegetation cover. Obsidian is very detectable at low percent coverage of the surface (~5%).
- This was a limited study designed to examine the spectral detectability of artifacts in mixtures with backgrounds in a single spectrum. The spatial distribution of a target material in an image is equally important in its detection. In fact, even if a target occurs at below the detection thresholds determined in this study, it may yet be detectable over multiple pixels.
- The distribution of a target in an image may increase the chances for detection. Therefore, the results of this study need to be combined with spatial analysis to determine artifact detection limits in multispectral images.
- In addition to the spectral and spatial analysis, day/night sets of thermal images may enhance detection of artifacts.

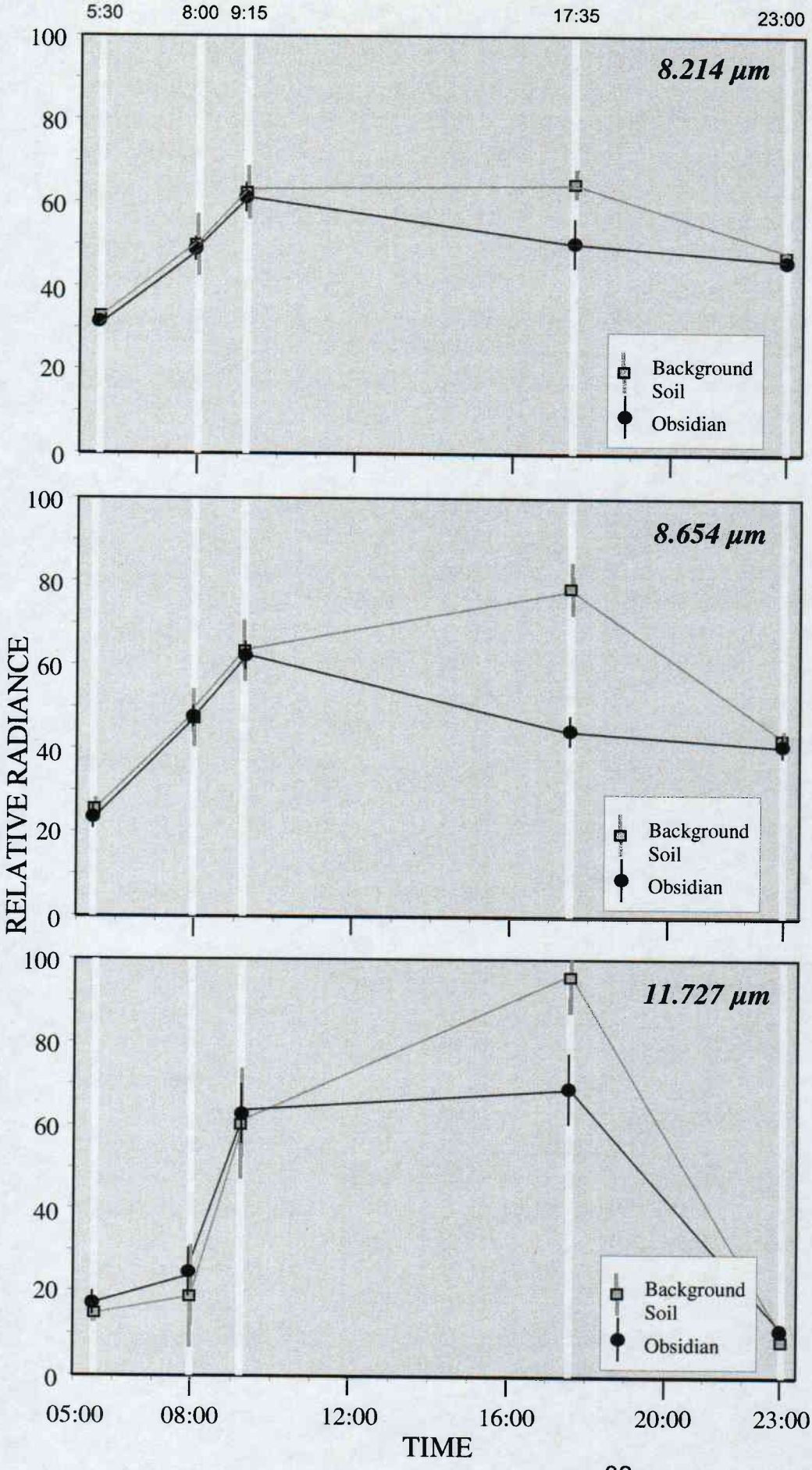

Figure 17: Change in radiance of obsidian and a background soil from 0500 hours until 2300 hours. The difference in the rate of heating and cooling of these materials is another potential approach for detecting artifacts.

Acknowledgements

This research was supported primarily by the U.S. Department of Defense through the Strategic Environmental Research and development Program (SERDP). This support was administered by the U.S. Army Research Office under research grant number DAAD-19-99-1-0261. The authors gratefully acknowledge the assistance of Elsa Abbott and Howard Tan of the Jet Propulsion Laboratory for technical assistance, John Issacson and Brad Vierra at LANL, and Carolyn Shepherd and Jan Lawson at CLNAWS. Thanks to Lynn Fenstermaker at DRI for assistance with the ASD instrument, and Ginger Vogler, Lycia Ronchetti, and Linda Piehl for administrative assistance. The authors also thank DRI for partial support for the research described here.

References Cited

Adams, J. B., M.O. Smith, and P.E. Johnson, 1986. Spectral mixture modeling: A new analysis of rock and soil types at the Viking Lander 1 site. *Journal of Geophysical Research* 91:B8, 8098-8112.

Adams, J.B. and McCord, T.B., (1971), Spectral reflectivity: optical properties of mineral separates, glass and anorthositic fragments from Apollo Mare samples, *Proc. Apollo 12 Lunar Sci. Conf.3, MIT Press, 2183-2190.*

Buck, P. E., S.C. Willis, and M.O. Smith, 1986a. A mixture modeling approach to remote sensing of archaeological sites in Egypt using Landsat imagery. Invited paper presented at Geological Society of America Annual Meeting, Archaeological Geology Division, San Antonio, Texas.

Buck, P. E., S.C. Willis, and M.O. Smith, 1986b. Application of multispectral imagery to Archaeological problems in arid lands: An Example from Egypt. Paper presented at 51st Annual Meeting of the Society for American Archaeology, New Orleans, April 1986.

Custer, J. F., T. Eveleigh, V. Klemas, and I. Wells, 1986. Application of Landsat data and Synoptic remote sensing to predictive models for prehistoric archaeological sites: An example from the Delaware coastal plain. *American Antiquity* 51:572-588.

Davis, P. A., G. L. Berlin, P.S. Chavez, Jr., 1987. Discrimination of altered basaltic rocks in the southwestern United States by analysis of Landsat Thematic mapper data. *Photogrammetric engineering and remote sensing* 53:45-58.

Ebert, J. I. and T. R. Lyons, 1983. Archaeology, anthropology, and cultural resource management. In *Manual of Remote Sensing*, 2nd edition, Vol. 2: 1233-1304. American Society of Photogrammetry.

Elston, R. G. and C.D. Zeir, 1984. The Sugarloaf obsidian quarry. Naval Weapons Center Administrative Publication 313, China Lake, California.

Elvidge, C. D., 1990. Visible and near infrared characteristics of dry plant materials. *International Journal of Remote Sensing* 11:1775-1795.

Gillespie, A.R., 1992. Spectral mixture analysis of multispectral thermal infrared images. *Remote Sens. Environ.* 42:137-145.

Gilreath, A. and W.R. Hildebrandt, 1997. Prehistoric Use of the Coso Volcanic Field.. Contributions of the University of California Archaeological Research Facility, No. 56. U.C. Berkeley.

Hewett, Edgar L.,1904. Archaeology of Pajarito Park, New Mexico. American Anthropologists n.s. 6(5):629-659.

Hewett, Edgar L., 1909, The Pajaritan Culture. American Journal of Archaeology 2nd series, 13(3):334-344.

Hewett, Edgar L., 1953 Pajarito Plateau and its Ancient People, 2nd ed. Revised. University of New Mexico Press. Albuquerque.

Hughes, R.E., 1988. The Coso volcanic field re-examined: Implications for obsidian sourcing And hydration dating research. *Geoarchaeology* 3(4):253-265.

Hunt, G. R., J. W. Salisbury, and C.J. Lenhoff, 1973. Visible and near infrared spectra of minerals and rocks: VII. Acidic igneous rocks. *Modern Geology* 4:217-224.

Hunt, G. R., and J. W. Salisbury, 1970. Visible and near infrared spectra of minerals and rocks: I. Silicate Minerals. *Modern Geology* 1:283-300.

Justice, C.O., J. R.. Townshend, B. N. Holbren, and C.J. Tucker, 1985. Analysis of the phenology of global vegetation using meteorological satellite data. *Int. Jour. Remote Sens.* 6:1271-1318.

Kahle, A. B. and A.F.H. Goetz, 1983. Mineralogic information from a new airborne thermal Infrared multispectral scanner. *Science* 222:24-27.

McDonald, E. V., S.L. Reneau and J.N. Gardner, 1996. Soil-forming processes on the Pajarito Plateau: Investigation of a soil chronosequence in Rendija Canyon. *New Mexico Geological Society, Guidebook*, p. 367-374.

Nash, D.B. and Conel, J.E., (1974), Spectral reflectance systematics for mixtures for powdered hypersthene, labradorite, and ilminite, *J. Geophys. Res.* 79:1615-1621.

Perkin-Elmer GmbH, 1991. Lambda 19 DM UV/VIS & UV/VIS/NIR Spectrometers. Instrument Manual. Perkin-Elmer publication B2153, release 1.1/Sept. 1991. D-7770 Uberlingen, Federal Republic of Germany.

Purtyman, W.D. and W.R. Kennedy, 1971. Geology and Hydrology of Mesita del Buey. Los Alamos National Laboratory Report LA-4460.

Reneau, S.L., and E.V. McDonald, 1996. Landscape history and processes on the Pajarito Plateau, Northern New Mexico. Guidebook for the 1996 Rocky Mountains Friends of the Pleistocene Field trip, September 1996, 183 p.

Sabol, D.E., J.B. Adams and M.O. Smith, 1992. Quantitative sub-pixel spectral detection of targets in multispectral images, *Jour. Geophys. Res.*, 97, E2, 2659-2672.

Singer, R.B. and McCord, T.B., (1979), Mars: Large scale mixing of bright and dark surface materials and implications for analysis of spectral reflectance, *Proc.10th Lunar Sci. Conf., 1835-1848.*

Steen, Charlie R., 1971. Pajarito Plateau Archaeological Survey and Excavations. Los Alamos Scientific Laboratory of the University of California Publication LASL-77-4. Los Alamos.

Stuart, David E., 1989. The Magic of Bandelier. Ancient City Press: Santa Fe, New Mexico.

Tucker, C.J., I.Y. Fung, C.D. Keeling, and R.H. Gammon, 1986. Relationship between atmospheric CO^2 variations and a satellite derived vegetation index. *Nature* 319:195-199.

Ustin, S.L., M.O. Smith, S. Jacquemoud, MM verstraete, and Y. Govarts, n.d. Geobotany: Vegetation mapping for earth sciences, In A. Rencz (Eds.) *Manual of Remote Sensing: Earth Sciences Volume*, chapter 4 in revision.

Vincent, R.K, 1997. *Fundamentals of geological and environmental Remote Sensing.*